Fatigue life of C-FRCM strengthened corroded RC continuous beams under multi-intervention system

Ran Feng [a], Pi-Yu Chen [a], Fangying Wang [b], Ying Xu [a], Ji-Hua Zhu [c*]

[a] *School of Civil and Environmental Engineering, Harbin Institute of Technology, Shenzhen, China (518055)*

[b] *Department of Civil Engineering, University of Nottingham, United Kingdom*

[c] *Guangdong Provincial Key Laboratory of Durability for Marine Civil Engineering, College of Civil and Transportation Engineering, Shenzhen University, Shenzhen, China (518060)*

Abstract

A new fatigue life prediction model for reinforced concrete (RC) beams is proposed. The model was applied to carbon-fabric reinforced cementitious matrix (C-FRCM) strengthened corroded RC beams under the impressed current cathodic protection (ICCP) and structural strengthening (SS) multi-intervention system. The stress development of steel bar in the fatigue process was captured by employing the fracture mechanics and finite element (FE) analysis. The concept of equivalent initial flaw size (EIFS) was also introduced to account for the actual initial micro crack size of steel bar. The feasibility of the model was validated through comparisons of the numerical deflection, the strain of steel bar and fatigue life of RC beams against the test results. The validated model was then used to examine the effects of key parameters including load level, corrosion degree of steel bar and polarization degree of C-FRCM on the fatigue life of RC beam. Furthermore, the results of the parametric study were used to fit *S-N* curve and analyse the reliability. The high accuracy of the model was shown to be suitable for the fatigue life prediction of ICCP-SS system in long-term service. It was also found that the fatigue life of the corroded RC beams was greatly improved through strengthening with C-FRCM.

Keywords: Carbon-fabric reinforced cementitious matrix (C-FRCM); Continuous beam; Corroded; Fatigue life; Multi-intervention system; Reinforced concrete (RC)

*Corresponding author.
E-mail address: zhujh@szu.edu.cn (J.-H. Zhu).

1. Introduction

The durability of reinforced concrete (RC) structures has always been an important topic in civil engineering research, among which steel bar corrosion has been found to be one of the most influential factors. The annual economic and social losses resulted from structural durability failures are huge [1, 2], costing 6.237 billion RMB in China in 2014 [3]. In response to the deterioration of the RC structures caused by the corroded steel bar, scholars have conducted extensive investigations into structural strengthening (SS) [4, 5] and impressed current cathodic protection (ICCP) [6-10] with carbon fiber reinforced polymer (CFRP). However, the resin in CFRP degrades during the service process in the conventional environment [11-13], resulting in decreasing in bearing capacity. Therefore, engineering and research interests have been turned towards using carbon fabric-reinforced cementitious matrix (C-FRCM) to strengthen RC structures [14-17]. Up to now, C-FRCM has been proven to be capable of strengthening RC structures with rather promising results [15, 18, 19]. However, C-FRCM degrades under the current and acid environment [20], where fatigue failure could happen abruptly under low loads in real service. This type of failure is difficult to detect and consequently causes unnecessary property losses and personal injuries. Investigation into fatigue life prediction of C-FRCM strengthened RC structures has become imperative and this is the focus of the current study.

Up to now, the study of fatigue life of corroded RC beams strengthened with CFRP has been rather limited, and those strengthened with C-FRCM have not been investigated. The previous studies have focused on the influence of fatigue stress amplitude, corrosion degree of steel bar and CFRP layers on fatigue life [21-23]. Overall, there are two methods for predicting the fatigue life of RC beams. The first method is based on the material damage model, which is capable of determining the fatigue life of the structures by observing the damage of the material according to the stress of the component [24]. The second method [25-27] is based on the crack development of the steel bar in the component, using fracture mechanics to calculate the life of the steel bar, thereby anticipating the fatigue life of the component. The second method has been found to be in better agreement with the real engineering cases, however, it ignores the stress development of steel bar in the fatigue process and therefore results in some deviations from the real fatigue scenarios.

Under the impressed current cathodic protection-structural strengthening (ICCP-SS) system,

the authors have studied the bending fatigue behaviour of corroded RC beams strengthened with C-FRCM [28]. In order to accurately evaluate the fatigue life of corroded RC beams strengthened with C-FRCM under ICCP-SS multi-intervention system, it is urgent to propose an appropriate fatigue life prediction model. Therefore, the aim of the current study is fourfold: first, to establish a fatigue life prediction model by using finite element (FE) modeling with the inclusion of fracture mechanics and the concept of equivalent initial flaw size (EIFS); second, to use DIANA software [29] to simulate results and validate the model by comparing the deflection, steel bar strain, fatigue life of the beam from the FE model with those from the tests; third, to use the validated model to study the effect of key structural parameters on fatigue life of corroded RC beams strengthened with C-FRCM, including the load level, corrosion degree of steel bar and polarization degree of C-FRCM; fourth, to use simulation results to fit the *S-N* curve, and use the Monte Carlo method [30] to analyse the reliability of the fatigue life from the probabilistic point of view.

2. A brief summary of experimental programme

An experimental programme was carried out by the authors to investigate the behaviour of RC beams strengthened by C-FRCM. A brief summary is introduced herein, and a full description of the tests is provided in Ref. [28]. A total of six RC continuous beams were designed for the experimental investigations, divided into two groups (see Table 1). The first group of unstrengthened uncorroded RC beams was subjected to static loading to determine the ultimate bearing capacity. In the second group, different types of RC beams were subjected to fatigue loading to obtain their fatigue performance. In Table 1, the label system was designed according to the types of RC beams and loading tests, separated by a hyphen. For example, the specimen label “B-S” represents unstrengthened uncorroded RC beams in static test, while “CSBP0-F” indicates the corroded RC beam strengthened with C-FRCM (the polarization degree was 0) was subjected to fatigue test.

The continuous beam was fabricated with a cross-sectional size of 150×250 mm (width×height) and a total length of 2400 mm with a clear length of single-span set as 1100 mm. The longitudinal steel bar and stirrups were made of HRB400 steel bar with diameters of 14 mm and 8 mm, respectively; both were hot-rolled ribbed steel bars with nominal yield strength of 400 MPa [31]. The spacing of the stirrups was 80 mm, and the specific layout is shown in Fig. 1. The continuous

beam was strengthened on the top surface of the mid-support and the bottom surface of the mid-span of the beam, as shown in Fig. 2, following the guidance from Chinese Code (CECS146: 2003) [32]. In addition, the 28-day average compressive strength of concrete was 27 MPa; the yield strength, ultimate strength and elastic modulus of 14 mm steel bar were 474.7 MPa, 628.7 MPa and 213.4 GPa, respectively, while those of 8 mm steel bar were 356.3 MPa, 479.5 MPa and 196.7 GPa; the flexural strength and compressive strength of cementitious matrix were 16.47 MPa and 67.24 MPa, respectively; the tensile ultimate stress, ultimate strain and elastic modulus of carbon fiber mesh were 1333 MPa, 1.126% and 118.4 GPa, respectively. Meanwhile, the mechanical properties of C-FRCM composites are summarised in Table 2.

3. Development and verification of fatigue life prediction model

Currently, the numerical simulation of RC beams under fatigue loading can be categorised into two methods [33]: the fatigue life analysis at the final stage and the fatigue life analysis over the whole process of fatigue loading. In the former method, material properties of the constitutive components are assumed to be the same over the whole fatigue process. Static analysis is conducted to obtain the stress and strain of the RC beam, and the location with the maximum stress (most prone to fatigue failure) of the RC beam under static loading. Then, combined with the fatigue life curve and structure load spectrum of the material, the fatigue life of the structure is obtained by using the damage accumulation rule. This method retains the simulation simplicity, however, only the final fatigue life can be obtained. Meanwhile, it also ignores the changes of material properties over the long-term fatigue loading process, which might result in unconservative predictions. To consider this effect, in the fatigue life analysis over the whole process of fatigue loading, an appropriate material damage model is defined and the fatigue process is divided into multiple stages. It is assumed that the material properties remain the same during each stage, however, updated between stages according to the material damage model. The fatigue performance as well as the final fatigue life of RC beams at various stages can thus be obtained. The second analysis method, though being more complex, is capable of simulating the fatigue performance of RC beams over the whole fatigue loading process, and therefore adopted herein to analyse the fatigue life of RC beams.

In simulating the mechanical properties of RC beams in the fatigue process, the accuracy of the results mainly depends on the selection of the fatigue damage model for each constituent material,

particularly for corroded steel bar due to their reduced cross-sectional area and local pitting corrosion. To eliminate the effect of stress concentration caused by the local pitting corrosion, an empirical corrosion correction coefficient was commonly used [34-36]. The method was initially attempted but found to result in a high level of disparity and inaccuracy for the examined RC beams with corroded steel bars. This is owing to the fact that the main failure mode of the examined RC beams was triggered by the fracture of steel bars. In the RC beams, the location and size of the pitting corrosion are highly discrete, the steel bar is very sensitive to initial defects under fatigue loading, therefore, small initial crack fluctuations may significantly influence the fatigue life of RC beams. In this study, in addition to the corrosion correction coefficient of steel bar, fracture mechanics was also used to study the fatigue crack propagation of steel bar to improve the accuracy of corroded steel bar damage model.

Fracture mechanics has been used widely [37] to calculate the crack growth rate of steel bar, and thereby predicting the fatigue life of RC beams. It is assumed that the stress of the steel bar remains constant during the fatigue stage and ignores the deterioration of concrete, which was not in agreement with the observation of the test results in the examined RC beams [28]. Therefore, to rectify this, the deterioration of material properties has been considered through adopting different material properties in separated stages over the whole fatigue loading process. In this study, the FE analysis was used in combination with the fracture mechanics analysis and considers the whole fatigue loading process. The fatigue stage is first simplified into several stages, assuming the material properties remain unchanged over each stage, but updated upon reaching the end of the stage according to the material damage model; then, a static load is applied to the RC beams to obtain the stress of the steel bar, and thereby the strain of the steel bar; this is to obtain the cracking development of the steel bar by using fracture mechanics; finally, the fatigue life of the RC beam is obtained through the predicted fatigue life of the steel bar on basis of the crack development.

DIANA (Displacement Analyzer) software [29] was used to analyse the whole fatigue process of RC beams, and the specific steps are as follows (see Fig. 3):

(1) The FE model of RC beam was established, and the initial constitutive equation of material was inputted.

(2) The static load of the beam was carried out, and the stress-strain results of the RC beam were outputted.

(3) Determine whether the component of RC beam fails or not, if fails, output the result and end the simulation. If not, the fatigue times (N) will be increased by ΔN. According to the stress-strain results, the fatigue properties of steel bar are calculated by fracture mechanics after N (N=N+ΔN) times fatigue loading, and fatigue properties of other material are calculated by material damage model after N times fatigue loading.

(4) Updating the constitutive relationship of materials in FE model.

(5) Repeat steps (2)-(4) until the RC structure fails.

3.1. Fatigue damage model of constituent materials

(1) Concrete

According to [33], the strength attenuation model of concrete is given by Eq. (1),

$$\frac{\delta_{r,c}(N)}{f_c} = \frac{x(N)}{a_d[x(N)-x(1)]^2 + x(N)} \tag{1}$$

where $\delta_{r,c}(N)$ is the residual strength of concrete under the N-th fatigue loading (MPa); f_c is the compressive strength of concrete (MPa); a_d is a constant related to the strength of concrete, and taken as 1.36 [38] herein; $x(N)$ is a function related to the fatigue loading times, which can be expressed as:

$$x(N) = \frac{\lg N}{\lg N_f}[x(N_f)\text{-}1]+1 \tag{2}$$

where $x(N_f)$ is a function related to the stress process of concrete, which can be expressed as:

$$x(N_f) = \frac{2\alpha_d\delta_{\max} + f_c - \delta_{\max} + \sqrt{(f_c-\delta_{\max})^2 + 4\alpha_d\delta_{\max}(f_c-\delta_{\max})}}{2\alpha_d\delta_{\max}} \tag{3}$$

where $\delta_{\max}$ is the maximum stress of concrete (MPa).

According to CEB-FIP specification [39], the fatigue life of concrete (N_i) is calculated as:

$$\begin{cases} \log N_1 = (12+16S_{\min}+8S_{\min}^2)(1-S_{\max}) \\ \log N_2 = 0.2\log N_1(\log N_1 - 1) \\ \log N_3 = \log N_2(0.3-0.375S_{\min})/\Delta S \end{cases} \tag{4}$$

$$\Delta S = |S_{\max}| - |S_{\min}| \tag{5}$$

where N_i is the fatigue life of concrete, i=1, 2, 3; $S_{\max}$ is the maximum load ratio of concrete; $S_{\min}$ is the minimum load ratio of concrete; ΔS is the magnitude of the load ratio on the concrete.

$$\log N_i = \begin{cases} \log N_1 \left(\log N_1 \le 6 \right) \\ \log N_2 \left(\log N_1 > 6, \Delta S \ge 0.3 - 0.375 \Delta S_{\min} \right) \\ \log N_3 \left(\log N_1 > 6, \Delta S < 0.3 - 0.375 \Delta S_{\min} \right) \end{cases} \tag{6}$$

Holmen [40] proposed the stress-strain curve of concrete under compressive fatigue loading, and fitted the concrete stiffness degradation model as follows through further experiments and theoretical research:

$$E_c^f \left(n \right) = \left(1 - 0.4 \frac{N}{N_i} \right) E_c \tag{7}$$

where $E_c^f(n)$ is the modulus of elasticity of concrete after n-th fatigue loads (MPa); E_c is the initial elastic modulus of concrete (MPa).

(2) Steel bar

The fatigue characteristics of steel bar are significantly different from those of concrete. Under fatigue loading, a small amplitude of cyclic softening or hardening will occur since the steel bar is still in the elastic stage. Under constant-amplitude fatigue loads, the steel bar inside the RC beam is generally under a relatively stable load range, so it can be assumed that the stiffness of the steel bar retains the same during the entire fatigue process.

The main influence of fatigue loading on the steel bar is on the most dangerous cross-section, which will undergo crack initiation, crack propagation and fracture. Upon the crack of steel bar developing to the critical size, the stress of steel bar is equal to its yield stress, and consequently the failure occurs. The failure criterion of steel bar is determined by Eq. (8):

$$\sigma_{s,\max} \ge f_y \tag{8}$$

$$\sigma_{s,\max} = \sigma_s \cdot A_s / A_s^f(n) \tag{9}$$

where $\sigma_{s,\max}$ is the maximum stress of the steel bar (MPa); A_s is the initial area of the steel bar (mm^2); σ_s is the stress of the steel bar (MPa); f_y is the yield stress of the steel bar (MPa); $A_s^f(n)$ is the area of the most dangerous cross-section of the steel bar after n cycles of cyclic loading (mm^2), which can be expressed as a crack related to Eq. (10):

$$A_s^f(n) = \frac{\pi D^2}{4} - \arccos\left(\frac{D/2 - a_n}{D/2} \right) \cdot \left(D/2 \right)^2 + \left(D/2 - a_n \right) \cdot \sqrt{\left(D/2 \right)^2 - \left(D/2 - a_n \right)^2} \tag{10}$$

where D is the initial diameter of the steel bar (mm); a_n is the length of the main crack of the steel bar after n cycles of cyclic loading (mm), calculated by implementing fracture mechanics, as detailed in the following Subsection 3.2.

(3) C-FRCM plate

C-FRCM plate is composed of carbon fiber mesh and cementitious matrix, in which the cementitious matrix acts as a binder. In the examined RC beams, C-FRCM plate was stuck on the tensile zone of RC beam and under tension in the whole loading process. In the FE model, the constitutive relationship of cementitious matrix was modelled by incorporating the measure values from material properties test into a predefined concrete model, considering their similarities in mechanical properties.

For carbon fiber bundle, Tanabe et al. [41] reported that the fatigue limit of carbon fiber is 80-90% of the static tensile strength, which indicates that the carbon fiber remain unbroken when the stress level is lower than 80% of the static tensile strength. In this study, the tensile strength of the carbon fiber was measured to be 1333 MPa, which is significantly greater than the tensile strength of the steel bar. Thus, the carbon fiber have no fatigue damage before the fracture of steel bar, and therefore the damage of carbon fiber during fatigue process was not considered and modelled in the numerical analysis.

In the experiments, the interface damages between concrete-mortar and mortar-fiber were not detected prior to the fatigue failure of the beams. This is primarily owing to the fact that interaction forces in the interfaces remained lower than the critical crack or debonding levels when the cyclic load was small (applied load ratio ranged from 0.1-0.7) during the whole fatigue loading process. Therefore, the influence of interface damages on fatigue life of RC beams was not considered and modelled.

3.2. Fracture mechanics analysis of steel bar

The crack development of the steel bar was obtained through the implementation of fracture mechanics analysis on the stress of steel bar from the numerical simulations. The aim is to determine the a_n values in Eq. (10).

(1) Fracture mechanics calculation

Cross-sectional imperfections of steel bar are inherent properties widely existed due to the influence of manufacturing process and corrosion, characterized by the defects in the steel bar. Under fatigue loading, the cracks of the steel bars develop from original defects, which trigger small cracks, and then develop into macro cracks until failure [27]. Each development can thus be

categorized into three main stages, i.e., crack initiation, crack propagation and crack break. For the crack growth rate in the second stage, it can be described by the Paris equation:

$$\frac{\mathrm{d}a}{\mathrm{d}N} = C\left(K_{\max} - K_{\min}\right)^m \tag{11}$$

where da/dN is the crack growth rate per cycle of fatigue loading (mm), in which a is the length of the crack gap (mm), and N stands for the N-th loading; $K_{\max}$ is the stress intensity factor corresponding to the upper limit of the load ($\mathrm{MPa}\sqrt{\mathrm{m}}$); $K_{\min}$ is the stress intensity factor corresponding to the lower limit of the load ($\mathrm{MPa}\sqrt{\mathrm{m}}$); C and m are the material constants, C=$10^{-12.43}$, m =2.6 [42].

In linear fracture mechanics, the strength of the stress distribution at the crack tip depends on the stress intensity factor K, which depends on the crack size, geometry and applied stress:

$$K = \sigma Y\sqrt{\pi a} \tag{12}$$

where σ is the applied stress (MPa); Y is the geometric shape factor.

For single-side notched specimens [43], Y can be calculated according to the following equation:

$$Y = 1.12 - 0.231\left(\frac{a}{D}\right) + 10.55\left(\frac{a}{D}\right)^2 - 21.72\left(\frac{a}{D}\right)^3 + 30.39\left(\frac{a}{D}\right)^4 \tag{13}$$

Substitute Eq. (13) into Eq. (11), the crack growth rate can be expressed as:

$$\frac{\mathrm{d}a}{\mathrm{d}N} = C\left(Y\Delta\delta\sqrt{\pi a}\right)^m \tag{14}$$

where $\Delta\delta$ is the stress amplitude (MPa). Integrate Eq. (14) to obtain the fatigue life ΔN when the crack develops from a_N to $a_{N+\Delta N}$:

$$\Delta N = \int_{a_N}^{a_{N+\Delta N}} \frac{1}{C\left(Y\Delta\delta\sqrt{\pi a}\right)^m} da \tag{15}$$

Eq. (15) can be used to calculate the crack length of steel bar $a_{N+\Delta N}$ after N-th cyclic loading when the stress amplitude is $\Delta\delta$, and then whether the steel bar fails can be determined by Eq. (8).

(2) Determine the equivalent initial crack length

In Eq. (15), when the steel bar undergoes the first cycle, the lower limit of integral a_N=a_0, where a_0 is the initial crack length and needs to be determined first. There are two ways to determine a_0: first, the a_0 inside the material has reached the level of macroscopic cracks, which can be directly determined by nondestructive testing, this situation is equivalent to that the material does

not go through the crack initiation stage and directly enters the crack propagation stage; second, the material has not yet formed macroscopic cracks at the beginning, and cannot be obtained by nondestructive testing. Equivalent initial flaw size (EIFS) is an equivalent crack length, which can replace the prediction of crack initiation and short crack growth propagation of steel bar [27, 44, 45]. At this time, EIFS can be used to replace the actual initial micro crack size of steel bar. In the EIFS method, the material itself and the initial defects due to corrosion are considered, and it is widely used in fatigue life assessment [46-48].

The development of steel bar cracks can be divided into three stages. The first is the crack formation stage, the short crack growth rate presents a disordered form. At this time, fatigue is a surface phenomenon, which is affected by surface roughness, surface damage and other factors. The dispersion of steel bar life is large, which is an important reason for the large dispersion of fatigue test results. The second is the crack growth stage, the crack growth shows regularity and can be calculated by Eq. (11), but the calculated result only includes the life of the crack growth stage, not the life of the crack formation stage. In EIFS method, a_0 is replaced by a_{EIFS}, and the fatigue life calculated by this method showed in a better agreement with the real fatigue life of the specimen [44, 46, 48-50]. The results of the fatigue test are used to inversely calculate the fatigue life process to obtain the a_{EIFS} of each specimen, as shown in Table 3.

3.3. FE model

(1) Modeling and element selection

The FE model, longitudinal steel bar, stirrup size, thickness of the concrete cover, etc. are consistent with the test RC beam size, and to avoid local damage at the loading point, steel plate pads are set at the loading point and the support, as shown in Fig. 4.

Both concrete and cementitious matrix adopt CHX60 solid element, as shown in Fig. 5a, which is composed of hexahedral elements with 20 nodes, with a total degree of freedom of 60. The 3×3×3 Gaussian integration in the body is adopted, which has good boundary adaptability and computational convergence. Steel bar and carbon fiber mesh adopt the embedded steel bar element in DIANA, in which the steel bar is simulated by bar element, which is shown in Fig. 5b; and carbon fiber mesh is simulated by grid element, as shown in Fig. 5c.

(2) Material properties

The constitutive relationship of concrete and cementitious matrix is selected from the "concrete and masonry structure type" in DIANA, in which the compression curve adopts the parabolic compression model, and the tension curve adopts the Hordijk tensile softening model [29]. The constitutive relationship of steel bar adopts the Von Mises model in "Reinforcement and Pile Foundation" in DIANA while carbon fiber mesh uses a linear elastic constitutive model. Besides, the bond slip of the steel bar-concrete interface is considered by using the bond slip steel bar constitutive model in DIANA.

Modifications to the constitutive relationship should be made after the steel bars are corroded. In this study, a model proposed by Wu and Yuan [34] is adopted, and the equations are as follows:

When $0 < \rho \leq 5\%$,

$$f_{yc} = f_{y0}(1\text{-}0.029\rho) \quad (16)$$

$$f_{uc} = f_{u0}(1\text{-}0.026\rho) \quad (17)$$

$$\delta_c = \delta_0(1\text{-}0.0575\rho) \quad (18)$$

$$\varepsilon_{yc} = \varepsilon_{y0}(1\text{-}0.0575\rho) \quad (19)$$

$$E_{uc} = E_{u0}(1\text{-}0.052\rho) \quad (20)$$

When $\rho > 5\%$,

$$f_{yc} = f_{y0}(1.175\text{-}0.064\rho) \quad (21)$$

$$f_{uc} = f_{u0}(1.18\text{-}0.062\rho) \quad (22)$$

$$\delta_c = \delta_0(1\text{-}0.0575\rho) \quad (23)$$

$$\varepsilon_{yc} = \varepsilon_{y0}(1\text{-}0.0575\rho) \quad (24)$$

$$E_{uc} = E_{u0}(0.895\text{-}0.03\rho) \quad (25)$$

where ρ is the corrosion degree of steel bar (%); E_{uc} is the nominal modulus of elasticity of corroded steel bar (MPa); E_{u0} is the nominal modulus of elasticity of uncorroded steel bar (MPa); f_{yc} is the yield strength of corroded steel bar (MPa); f_{y0} is the yield strength of uncorroded steel bar (MPa); δ_c is the nominal elongation of corroded steel bar; δ_0 is the nominal elongation of uncorroded steel bar; ε_{yc} is the ultimate strain of corroded steel bar and ε_{y0} is the ultimate strain of uncorroded steel bar.

In addition, the corrosion in the steel bar may decrease the bonding strength; to reflect it, the slip constitutive of the corroded steel bar was corrected according to Liang et al. [51]. As steel bar corrosion mainly affects the bonding strength in the shear direction and has little effect on that of normal direction, only the tangential stiffness is corrected.

$$\tau_u = \left(1.6 + 0.7\frac{c}{d} + 20\rho_{sv}\right)\eta'(\rho)\cdot f_t \quad (26)$$

$$s_u = \frac{23d\mathrm{e}^{-0.09957\rho}}{625} \tag{27}$$

$$\eta'(\rho) = \begin{cases} 1 + 0.9443\rho - 0.9584\rho^2 + 0.3461\rho^3 - 0.0447\rho^4 & \rho \le 3\% \\ 1.4822\rho^{-0.4235} & \rho > 3\% \end{cases} \tag{28}$$

where τ_u is the ultimate bonding strength of corroded steel bar (MPa); s_u is the ultimate slip of corroded steel bar (mm); c is the thickness of concrete cover (mm); ρ_{sv} is the reinforcement ratio of the concrete specimen; f_t is the tensile strength of concrete strength (MPa) and $\eta'(\rho)$ is the reduction coefficient of bonding strength.

Therefore, the shear stiffness modulus (E_t) is calculated as follows:

$$E_t = \frac{\tau_u}{s_u} \tag{29}$$

(3) Loading and boundary conditions

The FE model is modelled to mirror the boundary and loading conditions adopted in the experiments, i.e., five-point bending test. The steel plate padstones are set at the mid-span and support of the beam, and the load is applied by using the steel plate padstones. The bearings at both ends of the beam are sliding hinge bearings, and the middle is fixed hinge bearing, as shown in Fig. 4.

(4) Meshing

The model is divided into several regular regional meshes, and the quality of mesh affects the convergence of the model and the accuracy of the results. Molaioni et al. [52] studied cyclic behaviour of RC columns subjected to localized corrosion in the plastic hinge regions, the 300×300×1800 mm column was divided into 50×50×50 mm mesh, and the 1500×750×500 mm foundation concrete were divided into 100×100×100 mm mesh. Georgiou et al. [53] studied the effectiveness of seismic retrofitting of existing structures, the 250×500×3000 mm column was divided into 100×100×250 mm mesh. Furthermore, the static test simulation of specimen B-S was carried out with four mesh sizes to investigate the sensitivity of mesh size on the convergency and accuracy of the results. This prior study was conducted to decide upon an appropriate mesh size before fatigue test simulation. The examined sizes were 60×60×60 mm, 50×50×50 mm, 40×40×40 mm and 30×30×30 mm. The comparisons of varied mesh size on the ultimate load of the RC beam and the strain of steel bar at mid-span and mid-support are summarised in Table 4. It can be

observed that the mesh size of 50×50×50 mm achieved good agreement between test and FE results, while maintain computational efficiency, and was therefore adopted in the subsequence simulations.

3.4. Validation of FE model

(1) Comparison of beams deflection and steel bar strain

The accuracy of the FE model is verified by comparing the calculated results with the experimental results. From Table 5 and Fig. 6, it can be seen that the agreement between the model and the unstrengthened corroded beam is higher since the average tested and calculated deflection ratio $\Delta_{Test}/\Delta_{FE}$ is 1.081, which is lower than that of the unstrengthened uncorroded beam ($\Delta_{Test}/\Delta_{FE}$ was 1.128) and the strengthened corroded beam ($\Delta_{Test}/\Delta_{FE}$ was 1.129). For all the RC beams, when the cycle is 0, $\Delta_{Test}/\Delta_{FE}$ ranges from 0.971-1.095, indicating high agreement. $\Delta_{Test}/\Delta_{FE}$ increases gradually with the increase of cycle, while it gradually decreases when the cycle reaches 5,000. And when the cycle was 20 thousand, $\Delta_{Test}/\Delta_{FE}$ reduced to the range of 1.091-1.107.

Another comprehensive assessment is made from the mean value of $\varepsilon_{Test}/\varepsilon_{FE}$ and the coefficient of variation (COV) of the steel bar strain at the mid-span and the support (Tables 6-7 and Fig. 6). The agreement between the model and the unstrengthened corroded beam is higher since $\varepsilon_{Test}/\varepsilon_{FE}$ and COV at the mid-span were 1.036 and 0.035, respectively, which is lower than that of the unstrengthened uncorroded beam ($\varepsilon_{Test}/\varepsilon_{FE}$ was 1.082, COV was 0.009) and the strengthened corroded beam ($\varepsilon_{Test}/\varepsilon_{FE}$ was 1.041, COV was 0.032). Besides, $\varepsilon_{Test}/\varepsilon_{FE}$ and COV at the support of unstrengthened corroded beam are still better than that of the unstrengthened uncorroded beam and strengthened corroded beam. For all RC beams, when the cycle is 0, $\varepsilon_{Test}/\varepsilon_{FE}$ ranges at the mid-span and the support are 0.941-1.072 and 0.723-1.027, respectively. $\varepsilon_{Test}/\varepsilon_{FE}$ increases gradually with the increase of cycle, while it began to decrease gradually when the cycle reaches 5,000. For unstrengthened beams, when the cycle is 10 thousand, the steel bar strain ratio $\varepsilon_{Test}/\varepsilon_{FE}$ at the mid-span and the support of the uncorroded beam are 1.073 and 0.951, respectively; while that of the corroded beam is 1.033 and 1.023, which indicates that the model has higher accuracy for the simulation of the steel bar strain of the corroded beam. For strengthened corroded beams, when the cycle is 10 thousand, the steel bar strain at the mid-span of the specimens SCBP0-F, SCBP1-F and SCBP2-F are 1.142, 1.079 and 0.999, respectively; and the steel bar strain at the support of the specimens SCBP0-F and SCBP1-F are 0.974 and 1.022, respectively. Therefore, with the increase

of C-FRCM polarization degree, the $\varepsilon_{Test}/\varepsilon_{FE}$ keeps approaching unit, and the accuracy of the model becomes higher. It should be noted that when the cycle is 20 thousand, the test data of specimens B-F, CB-F and CSP2B-F are missing, so the data comparison and analysis of different types of specimens will not be carried out. In general, the steel bar strain of the FE model is in good agreement with the test results. It was found that the model shows better applicability to unstrengthened corroded beams, compared to unstrengthened uncorroded beams, and it also revealed that better agreement to the tests was achieved for higher C-FRCM polarization degree.

(2) Comparison of fatigue life

According to the stress of the steel bar obtained from the FE model, the fatigue life of the RC beam at the fracture of the steel bar is calculated according to Eqs. (6) and (13). The numerical and experimental values are compared in Table 8. It can be seen that the ratio of N_{Test}/N_{FE} ranging from 0.885 to 0.963, the mean value is 0.915 with a corresponding COV of 0.031, indicating that the FE model is capable of replicating the test results with high consistency for all the uncorroded beams, corroded beams, as well as C-FRCM strengthened corroded beams. This may be owing to the introduction of EIFS, which closely represent the fatigue life of steel bar with initial defects. In addition, the model is most consistent with the prediction of the life of unstrengthened corroded beams, with N_{Test}/N_{FE} of 0.963. For strengthened corroded RC beams, when the polarization degree of C-FRCM is 0, N_{Test}/N_{FE} is 0.890; with the increase of polarization degree, the life prediction coefficient increases gradually. When the polarization degree is 2, the life prediction coefficient is 0.923, which is more consistent with the test results.

The FE model is also verified against existing experimental results on RC beams under fatigue loading in the literature. Song and Yu [24] and Al-Hammoud et al. [21] examined the fatigue performance of corroded RC beams strengthened with CFRP sheets. The key test results, including corrosion degree, fatigue life, minimum and maximum fatigue load, applied load ratio and strengthening status are summarised in Table 9. The graphical comparisons of the prediction and the test results are displayed in Fig. 7. It can be seen that most of the data points are within the confidence interval of 0.13, which indicates that the proposed model is capable of predicting the fatigue life of strengthened corroded RC beams.

4. Parametric study

The validated fatigue life prediction model was utilized to conduct the parametric study. Based on the analysis of the test results and previous studies [28], the load level, corrosion degree of steel bar and C-FRCM polarization were studied as key variables that affect the fatigue life of RC beams. The load levels are 0.2, 0.3, 0.4, 0.5 and 0.6 times of the ultimate bearing capacity of RC beam, and the stress ratio is the same as that adopted in the test program, taking 0.2. It can be seen from the test program that when corrosion degree of steel bar is 0, a_{EIFS} is 0.890; when the corrosion degree of the corroded beam is 3.17-3.85%, a_{EIFS} is 0.992-1.297. Beyond corrosion degree of 3.85%, a_{EIFS} is not available. To facilitate the investigation beyond this corrosion degree, a linear interpolation was undertaken and a value of a_{EIFS} is assumed to be 1.40 at a corrosion degree of 7%. The polarization degree of C-FRCM is consistent with the test program, and the polarization degree is 0, 1 and 2. In addition, an unstrengthened beam is added as a reference, therefore, a total of 60 specimens were selected for parametric study, as shown in Table 10.

The specimens are labeled according to beam type and the loading level, for example, the specimen label “C0B-L0.2” represents that RC beams with a corrosion degree of 0, and subjected to cyclic loading at a load level of 0.2, while “C3.5SP1B-L0.2” indicates that RC beams with a corrosion degree of 3.5% strengthened by a C-FRCM with a polarization degree of 1, and subjected to cyclic loading at a load level of 0.2.

4.1. S-N curve

The power function is used to describe the load amplitude and fatigue cycle *S-N* curve:

$$S^{m'}N = C' \tag{30}$$

where *m'* and *C'* are the parameters related to materials, stress ratios, and their values are obtained by regression analysis on test data, *S* is defined as the load amplitude:

$$S = P_{\max} - P_{\min} \tag{31}$$

where $P_{\max}$ is the upper limit of load (kN); $P_{\min}$ is the lower limit of load (kN).

The *S-N* curve expression (see Table 11) is obtained through regression analysis, from which it can be seen that the logarithm of the load amplitude and the logarithm of the fatigue life are basically linear; besides, the coefficient of determination R^2 ranges from 0.954 to 0.984, and the dispersion is rather small, indicating that the *S-N* curve expression is accurate and acceptable.

It can be seen from Table 10 and Fig. 8 that as the load amplitude continues to increase, the

fatigue life of the beam is decreasing gradually. Under a load level of 0.2, the fatigue life of the specimen C0B is 1,580,759 times, and the fatigue life of the specimen C0SP0B is 2,590,252 times, the use of C-FRCM strengthening increases the fatigue life of the beam by approximately 63.9%; when the load level is 0.6, the fatigue life of the specimen C0SP0B is 125.5% of the specimen C0B. This is attributed to the reason that C-FRCM bears the tensile stress of the steel bar during the fatigue process, which improves the fatigue life of the beam. It is worth noting that the fatigue life of all types of C-FRCM strengthened beams is higher than the corresponding unstrengthened beams, indicating that C-FRCM strengthening can significantly improve the resistance of beams to fatigue load.

4.2. The effect of load level on fatigue life

Based on the fatigue life of beams at 0.2 load level, the changes of fatigue life of beams under different load levels were compared. It can be seen from Table 12 and Fig. 8 that, the load level plays a key role in the fatigue life of the beam, as also documented in previous studies [22, 24, 54, 55]. For all types of beams, when the load level rises from 0.2 to 0.3, the fatigue life quickly drops to 59.2-65.8%; as the load level continues to rise, the fatigue life continues to decline. When the load level rises to 0.6, the fatigue life is reduced to 8.2-10.4% (134,165-206,855 times), for unstrengthened beams, on the verge of a dangerous state of fatigue damage. These results indicate that the fatigue life of the beam decreases gradually with the increase of the load level. Therefore, to reduce the possibility of fatigue failure of the beam, the load level should be lower than 0.6 of the ultimate static strength.

4.3. The influence of corrosion degree of steel bar on fatigue life

Based on the fatigue life of beams without corrosion degree of steel bar, the changes of fatigue life of beams with different corrosion degrees were compared (see Table 13). It can be seen from Table 13 and Fig. 9 that as the corrosion degree continues to increase, the fatigue life of the beam continues to decrease, since the higher the corrosion degree of steel bars, the smaller the effective area of steel bars, which intensifies the stress concentration. When the corrosion degree increases from 0 to 3.5%, the fatigue life of unstrengthened beams and C-FRCM strengthened beams are significantly reduced to 64.8-75.8% and 72.6-81.2%, respectively. When the corrosion degree of

steel bars continues to increase to 7%, the fatigue life of unstrengthened beams and C-FRCM strengthened beams decreases to 47-57.8% and 59.6-63.9%, respectively. In general, the fatigue life of beams is approximately linear with the corrosion degree of steel bar; meanwhile, the effect of steel bar corrosion on the fatigue life of unstrengthened beams is significantly greater than that of C-FRCM strengthened beams. This also reveals that C-FRCM can effectively increase the fatigue life of RC beams despite the negative influence from the steel bar corrosion.

4.4. The effect of polarization degree of C-FRCM on fatigue life

With reference to the fatigue life of beams with C-FRCM polarization degree of 0, the fatigue life of beams with different polarization degrees were compared. The statistical comparisons are presented in Table 14, along with a graphical comparison in Fig. 10. It can be seen that with the increasing polarization degree, the fatigue life of the beam decreases continuously and slightly. The reason for the decrease in fatigue life can be attributed to the fact that the polarization of the C-FRCM plate causes acidification [25, 56], and the cementitious matrix deteriorates under electrified conditions. Therefore, the bonding force between the cementitious matrix and the carbon fiber interface decreases [20], and the tensile stress taken by C-FRCM decreases. It was noticed that when the polarization degree increases from 0 to 1, the fatigue life of the beam decreases to 83.4-95.9%; and when the polarization degree continues to increase to 2, the fatigue life of the beam decreases to 77.1-92%. In general, the polarization degree of C-FRCM plate showed to be less influential on the fatigue life.

5. Reliability analysis

In reliability design, reliability is usually a function of time, denoted as $R(t)$, where t is a certain moment. In this paper, the cycle is used instead of time, so the reliability function is denoted as $R(n)$, where n represents a certain cycle. The random variable N represents the cycle of structure from starting to failure, and the reliability of the structure at the n-th cycle is expressed as:

$$R(n)=P(N>n) \tag{32}$$

When n=0, the reliability is 1, and as the cycle increases, the reliability gradually decreases.

5.1. Operation steps of Monte Carlo method

Assuming that the number of random simulations is N, and the number of failures is F, the approximate value of the total failure probability is F/N. The calculation steps are as follows:

(1) Determine the limit state equation when a component or structure fails.

(2) Determine the function distribution of each random variable in the limit state equation.

(3) According to the probability distribution function of the random variable, a random number is generated and substituted into the limit state equation. This step is repeated N times.

(4) Calculate failure probability according to the result of step (3).

5.2. Limit state equation

According to the limit state of the structure, the corresponding limit state function is established, which can be expressed as the equation of various random variables:

$$Z=g(X)=g(X_1, X_2,..., X_n) \tag{33}$$

When there are only random variables R and S, Z can be expressed as (R means resistance, S means action effect):

$$Z=g(R, S)=R-S \tag{34}$$

When $Z>0$, the structure is in the reliable state; when $Z=0$, the structure is in the limit state; when $Z<0$, the structure is in the failure state.

Based on the Paris equation and referring to [48], the limit state equation of the beam is established from the perspective of fracture mechanics, and then derived from Eq. (14):

$$\int_{a_0}^{a_c} \frac{1}{C\left(Y\sqrt{\pi a}\right)^m} da = C \cdot N \cdot (\Delta\delta)^m \tag{35}$$

If the stress of the steel bar $\Delta\delta$ remains constant throughout the fatigue process, the total fatigue life of the specimen is:

$$N = \int_{a_0}^{a_c} \frac{1}{C\left(Y\Delta\delta\sqrt{\pi a}\right)^m} da \tag{36}$$

Then the limit state equation for the failure of the specimen between cycles [0, N_f] can be expressed as:

$$g(\boldsymbol{X}) = N - N_f = \int_{a_0}^{a_c} \frac{1}{C\left(Y\Delta\delta\sqrt{\pi a}\right)^m} da - N_f \tag{37}$$

According to Chinese Code (GB/T 50152-2012) [57] and test [28], after (1, 5, 10, 30, 50, 100, 200, 300, 500, 700, 1000, 1500 and 2000) thousand times cycle of loading, respectively, the

constitutive relationship of the material is updated and the stress of the steel bar changes. The damage equation is defined as:

$$\varphi(a)=\int_{a_0}^{a}\frac{1}{\left(Y\sqrt{\pi a}\right)^m}da \tag{38}$$

Assuming that the cycle experienced by the equivalent initial crack length of the steel bar from a_0 to a_1 is N_1, then

$$\varphi(a_1)-\varphi(a_0)=CN_{up}^{1}(\Delta\delta_0)^m \tag{39}$$

$$\varphi(a_c)-\varphi(a_1)=CN_1(\Delta\delta_1)^m \tag{40}$$

$$\varphi(a_c)-\varphi(a_0)=CN_1(\Delta\delta_1)^m+CN_{up}^{1}(\Delta\delta_0)^m \tag{41}$$

$$N_1=\frac{\varphi(a_c)-\varphi(a_0)}{C(\Delta\delta_1)^m}-\left(\frac{\Delta\delta_0}{\Delta\delta_1}\right)^m N_{up}^{1} \tag{42}$$

$\Delta\delta_0/\Delta\delta_1$ represents the influence of updating the constitutive relation of material on the stress of steel bar, after N_2 cycles, the material is updated again:

$$N_2=\frac{\varphi(a_c)-\varphi(a_0)}{C(\Delta\delta_2)^m}-\left(\frac{\Delta\delta_0}{\Delta\delta_2}\right)^m N_{up}^{2} \tag{43}$$

By analogy, the j-th is:

$$N_j=\frac{\varphi(a_c)-\varphi(a_0)}{C(\Delta\delta_j)^m}-\sum_{i=1}^{j-1}\left(\frac{\Delta\delta_0}{\Delta\delta_j}\right)^m N_{up}^{i} \tag{44}$$

Therefore, the limit state equation for the fatigue failure of the beam at [0, N] during the entire fatigue process is:

$$g(X)=N_{up}^{1}+N_{up}^{2}+\cdots+N_{up}^{j}+N_j-N \tag{45}$$

5.3. Random variables

According to the limit state equation, the random variables mainly include: equivalent initial crack length a_{EIFS}, C, m, shape factor Y and stress amplitude. Lee and Cho [48] made statistics of a large number of experimental results and found that when m is used as a variable, its effect on the results can be ignored; a_{EIFS} conforms to the exponential distribution, and its COV is 1; C, Y and stress amplitude are in accordance with logarithmic distribution, and the COVs are 0.2, 0.1 and 0.1, respectively.

5.4. Random number generation

Random numbers are generated by pseudo-random number method, which requires two steps: the first is to generate uniformly distributed random numbers between (0, 1), and the second is to transform the random number generated in the first step into the random number obeying the distribution according to the distribution form of the random variable.

5.5. Reliability analysis of fatigue life

Generally, the number of samples taken in the actual project is 10,000, so the number of samples taken in this study is 10,000. According to the density distribution function of random variables and the limit state equation, the reliability of specimens at 50,000th, 100,000th, 200,000th, 500,000th, 1 millionth, 1.5 millionth, and 2 millionth cycles can be calculated by inputting the values of relevant variables under different cycles. Noting that fatigue fracture occurred before the fatigue cycle of the specimen CB-S0 reached 260,000 times in the test, so the data of the steel bar after 500,000 times was not obtained. According to the previous results [28], the stress amplitude of the steel bar did not change significantly in the later stage. Guo et al. [47] shows that the corrosion rate of steel bar in RC beam was 0-7.67%, and when the fatigue cycles were 0.43-1.18 million, the difference between initial stress and final stress of steel bar is 0-0.096%. Thus, it has been assumed that the stress amplitudes of the steel bar at the 500,000, 1 million, 1.5 million, and 2 million cycles remained to be the same level at that of the 200,000th cycle. After obtaining the stress data of the steel bars at different stages, the reliability was then calculated by employing Eq. (45).

It can be seen from Table 15 and Fig. 11 that the change trend of the reliability-cycle curve of all specimens are the same. As the cycle increases, the reliability continues to decrease. The fatigue life reliability of C-FRCM strengthened beams is significantly higher than that of unstrengthened beams, especially for corroded specimens. Under the load level of 0.2 and the cycle of 2 million, the reliability of the specimen C3.5B-L0.2 was 0.358, while that of the specimens C3.5SP0B-L0.2, C3.5SP1B-L0.2 and C3.5SP2B-L0.2 were 0.564, 0.521 and 0.532, respectively. Compared to the specimen C3.5B-L0.2, a significant increase up to 157.5%, 145.6% and 148.6% was respectively achieved, indicating that C-FRCM strengthening is able to greatly improve the fatigue life of the examined RC beams. The load level significantly influenced the results in reliability analysis, as shown in Fig. 11; the reliability of unstrengthened beam and C-FRCM strengthened beam was

mainly separated into two parts based on the specimens C0B-L0.4 and C0SP0B-L0.4. The upper part corresponds to the small load levels of (0.2-0.3), and the lower part corresponds to the large load levels of (0.4-0.6). As the cycle increased, the fatigue life reliability of large-load level specimens decreased rather rapidly, while that of small-load level specimens decreased slightly. Meanwhile, the reliability of small-load level specimens was significantly higher than that of large-load level specimens. It has been found that the corrosion degree of steel bar also played an important role in the fatigue life reliability of the RC beams. As the corrosion degree of steel bar continued to increase, the reliability gradually decreased. Under the load level of 0.4, when the cycle was 1 million, the reliability of the specimens C0SP0B-L0.4, C3.5SP0B-L0.4 and C7SP0B-L0.4 were 0.293, 0.225 and 0.157, respectively. Besides, increasing the polarization degree of the C-FRCM plate caused a slight decrease in the reliability of the fatigue life of the beam. Interestingly, increasing polarization made the reliability of specimens with different corrosion degrees closer to each other under the same load level, which intensifies the influence of load level on fatigue life reliability.

6. Conclusions

A new fatigue life prediction model of RC beams based on fracture mechanics and finite element analysis was proposed, as the stress development of steel bar in the fatigue process has an important impact on fatigue life. The concept of equivalent initial flaw size (EIFS) was also introduced to the model to account for the actual initial micro crack size of steel bar. The model was verified by comparing the deflection, steel bar strain and fatigue life of RC beams with the experimental results. The results showed that the deflection and steel bar strain of the beam were in good agreement with the experimental results.

The validated model was used to study the effect of load level, corrosion degree of steel bar and polarization degree of C-FRCM on fatigue life. The numerical results showed that C-FRCM has a significant strengthening effect on the beam, and effectively improves the fatigue life of the beam; under the load level of 0.2, the fatigue life of the specimen C0SP0B was 163.9% of that of the specimen C0B. From the results in the parametric studies on key structural factors, the load level was found to be the most influential factor affecting the fatigue life of the examined RC beams. With the increase of the load level, the fatigue life decreased rapidly; when the load level reached

to 0.6, the fatigue life decreased to 8.2-10.4% of those with the load level of 0.2. Therefore, it is suggested that, the load level should be lower than 0.6 of the ultimate static strength to mitigate the possibility of fatigue failure. In addition, the corrosion degree of steel bar was found to have an important influence on the fatigue life of the RC beams, and the relationship between them was approximately linear; when the corrosion degree increases to 7%, the fatigue life of C-FRCM strengthened beams decreases to 59.6-63.9% of those with the corrosion degree of 0. In addition, the polarization degree of C-FRCM plate showed to be less influential on the fatigue life of the RC beams; when the polarization degree was 2, the fatigue life of the beam was 77.1-92% of those with the polarization degree of 0. In the study, the load amplitude and fatigue cycle *S-N* curve expression with little discreteness was obtained by fitting the *S-N* curve of the parametric study results. In addition, the Monte Carlo method was used to analyse the reliability of the RC beams. The results showed that the factors for the reliability of RC beams fall in the order of load level, corrosion degree of steel bar and polarization degree of C-FRCM, which were well in line with the results of the parametric studies.

Acknowledgements

The authors are grateful for the financial support from Key-Area Research and Development Program of Guangdong Province (Grant No. 2019B111107002), National Key Research and Development Program of China (Grant No. 2018YFE0124900), National Natural Science Foundation of China (Grant Nos. 52178131/51538007/51778370/51861165204/51778191/ 52078173), Natural Science Foundation of Guangdong Province (Grant Nos. 2018A030313208/2017B030311004), Shenzhen Science and Technology Program (Grant No. GXWD20201230155427003-20200804174353001), Shenzhen Key Laboratory Launching Project (Grant No. ZDSYS20200810113601005).

Data availability statement

The raw/processed data required to reproduce these findings cannot be shared at this time as the data also forms part of an ongoing study.

References

[1] Delatte N. Failure, Distress and Repair of Concrete Structures. Elsevier; 2009.

[2] Pacheco-Torgal F, Melchers R, de Belie N, Shi X, Van Tittelboom K, Perez AS. Eco-Efficient Repair and Rehabilitation of Concrete Infrastructures. Woodhead Publishing; 2017.

[3] Hou BR, Li XG, Ma XM, Du CW, Zhang DW, Zhang M, Xu WC, Lu DZ, Ma FB. The cost of corrosion in China. npj Materials Degradation 2017; 1(1): 1-10.

[4] Azam R, Soudki K, West JS, Noël M. Strengthening of shear-critical RC beams: Alternatives to externally bonded CFRP sheets. Construction and Building Materials 2017; 151: 494-503.

[5] Colajanni P, Fossetti M, Macaluso G. Effects of confinement level, cross-section shape and corner radius on the cyclic behavior of CFRCM confined concrete columns. Construction and Building Materials 2014; 55: 379-389.

[6] Zhu JH, Zhu MC, Han NX, Liu W, Xing F. Electrical and mechanical performance of carbon fiber-reinforced polymer used as the impressed current anode material. Materials 2014; 7(8): 5438-5453.

[7] Lambert P, Van Nguyen C, Mangat PS, O'Flaherty FJ, Jones G. Dual function carbon fibre fabric strengthening and impressed current cathodic protection (ICCP) anode for reinforced concrete structures. Materials and Structures 2015; 48(7): 2157-2167.

[8] Nguyen CV, Lambert P, Mangat P, O'Flaherty F, Jones G. The performance of carbon fibre composites as iccp anodes for reinforced concrete structures. International Scholarly Research Notices 2012; 2012: 9.

[9] Zhu JH, Guo GP, Wei LL, Zhu MC, Chen XC. Dual function behavior of carbon fiber-reinforced polymer in simulated pore solution. Materials 2016; 9(2): 103-114.

[10] Zhu JH, Wei LL, Guo GP, Zhu AZ. Mechanical and electrochemical performance of carbon fiber reinforced polymer in oxygen evolution environment. Polymers 2016; 8(11): 393-405.

[11] Czaderski C, Martinelli E, Michels J, Motavalli M. Effect of curing conditions on strength development in an epoxy resin for structural strengthening. Composites Part B: Engineering 2012; 43(2): 398-410.

[12] Zhou YW, Fan ZH, Du J, Sui LL, Xing F. Bond behavior of FRP-to-concrete interface under sulfate attack: An experimental study and modeling of bond degradation. Construction and

Building Materials 2015; 85: 9-21.

[13] Zhu JH, Chen PY, Su MN, Pei C, Xing F. Recycling of carbon fibre reinforced plastics by electrically driven heterogeneous catalytic degradation of epoxy resin. Green Chemistry 2019; 21(7): 1635-1647.

[14] Ebead U, Shrestha KC, Afzal MS, El Refai A, Nanni A. Effectiveness of fabric-reinforced cementitious matrix in strengthening reinforced concrete beams. Journal of Composites for Construction, ASCE 2017; 21(2): 04016084.

[15] El-Maaddawy T, El Refai A. Innovative repair of severely corroded t-beams using fabric-reinforced cementitious matrix. Journal of Composites for Construction, ASCE 2016; 20(3): 04015073.

[16] Elghazy M, El Refai A, Ebead U, Nanni A. Effect of corrosion damage on the flexural performance of RC beams strengthened with FRCM composites. Composite Structures 2017; 180: 994-1006.

[17] Su MN, Wei LL, Zhu JH, Ueda T, Guo GP, Xing F. Combined impressed current cathodic protection and FRCM strengthening for corrosion-prone concrete structures. Journal of Composites for Construction, ASCE 2019; 23(4): 04019021.

[18] American Concrete Institute. Guide to Design and Construction of Externally Bonded Fabric-Reinforced Cementitious Matrix (FRCM) Systems for Repair and Strengthening Concrete and Masonry Structures. ACI 549.4 R-13. Farmington Hills, MI, USA, 2013.

[19] Pino V, Hadad HA, Basalo FDCY, Nanni A, Ebead UA, Refai AE. Performance of FRCM-strengthened RC beams subject to fatigue. Journal of Bridge Engineering, ASCE 2017; 22(10): 04017079.

[20] Chen PY, Pei C, Zhu JH, Su MN, Xing F. Sustainable recycling of intact carbon fibres from end-of-service-life composites. Green Chemistry 2019; 21(17): 4757-4768.

[21] Al-Hammoud R, Soudki K, Topper TH. Fatigue flexural behavior of corroded reinforced concrete beams repaired with CFRP sheets. Journal of Composites for Construction, ASCE 2011; 15(1): 42-51.

[22] Wang X, Sayed AM, Wu ZS. Modeling of the flexural fatigue capacity of RC beams strengthened with FRP sheets based on finite-element simulation. Journal of Structural Engineering, ASCE 2015; 141(8): 04014189.

[23] Masoud S, Soudki K, Topper T. CFRP-strengthened and corroded RC beams under monotonic and fatigue loads. Journal of Composites for Construction, ASCE 2001; 5(4): 228-236.

[24] Song L, Yu ZW. Fatigue performance of corroded reinforced concrete beams strengthened with CFRP sheets. Construction and Building Materials 2015; 90: 99-109.

[25] Correia JAFO, Blasón S, Jesus AMPD, Canteli AF, Moreira PMGP, Tavares PJ. Fatigue life prediction based on an equivalent initial flaw size approach and a new normalized fatigue crack growth model. Engineering Failure Analysis 2016; 69: 15-28.

[26] Ma YF, Xiang YB, Wang L, Zhang JR, Liu YM. Fatigue life prediction for aging RC beams considering corrosive environments. Engineering Structures 2014; 79: 211-221.

[27] Sun JZ, Ding ZH, Huang Q. Corrosion fatigue life prediction for steel bar in concrete based on fatigue crack propagation and equivalent initial flaw size. Construction and Building Materials 2019; 195: 208-217.

[28] Feng R, Wang J, Zhu JH, Dong ZJ. Fatigue behavior of corroded reinforced concrete continuous beams with multi-intervention system. Engineering Structures 2021; 231: 111748.

[29] Manie JKW. DIANA Finite Element Analysis, Release 9.4.4 User's manual. TNO DIANA BV, Delft, The Netherlands, 2014.

[30] Rubinstein RY, Kroese DP. Simulation and the Monte Carlo Method. John Wiley & Sons; 2016.

[31] Chinese Code. Steel for Reinforced Concrete Part 2: Hot Rolled Ribbed Bars. GB/T 1499.2-2018. Beijing: China Standard Press, 2018. (in Chinese)

[32] Chinese Code. Technical Specification for Strengthening Concrete Structures with Carbon Fiber Reinforced Polymer Laminate. CECS146: 2003, Beijing: China Planning Press, 2015. (in Chinese)

[33] Zhu JS, Zhu XC. Study on simplified method for the analysis of fatigue failure process of RC bridges. Engineering Mechanics 2012; 29(5): 107-114. (in Chinese)

[34] Wu Q, Yuan YS. Experimental study on the deterioration of mechanical properties of corroded steel bars. China Civil Engineering Journal 2008; 41(12): 42-47. (in Chinese)

[35] Ma YF, Xiang YB, Wang L, Zhang JR, Liu YM. Fatigue life prediction for aging RC beams considering corrosive environments. Engineering Structures 2014; 79(15): 211-221.

[36] Fernandez I, Bairán JM, Marí AR. Corrosion effects on the mechanical properties of

reinforcing steel bars. Fatigue and σ–ε behavior. Construction and Building Materials 2015; 101: 772-783.

[37] Brata TM. Fatigue Model for Prestressed Concrete Decks. Master thesis, Delft University of Technology, Delft, The Netherlands, 2016, 12-15.

[38] Chinese Code. Code for Design of Concrete Structures. GB 50010-2010, Beijing: China Architecture & Building Press, 2015. (in Chinese)

[39] CEB-FIP Model Code 1990. London: Euro-International Committee for Concrete.1993: 32-43.

[40] Holmen JO. Fatigue of concrete by constant and variable amplitude loading. Special Publication 1982; 75: 71-110.

[41] Tanabe Y, Yoshimura T, Watanabe T, Hiraoka T, Ogita Y, Yasuda E. Fatigue of C/C composites in bending and in shear modes. Carbon 2004; 42(8-9): 1665-1670.

[42] Zeng H. Study on Fatigue and Fracture Properties of Corroded Steel Bars. Master thesis, Central South University, Changsha, China, 2014, 62-63. (in Chinese)

[43] Krausz K, Krausz AS. On the physical meaning of the Paris equation. International Journal of Fracture 1988; 36(2): R23-R28.

[44] Zhan WG. Fatigue Life Prediction based on Crack Propagation with Application in Crane Metallic Structure. Doctoral dissertation, Harbin Institute of Technology, Harbin, China, 2015, 64-65. (in Chinese)

[45] Kaynak C, Ankara A, Baker TJ. A comparison of short and long fatigue crack growth in steel. International Journal of Fatigue 1996; 18(1): 17-23.

[46] Ma YF, Guo ZZ, Wang L, Zhang JR. Probabilistic life prediction for reinforced concrete structures subjected to seasonal corrosion-fatigue damage. Journal of Structural Engineering, ASCE 2020; 146(7): 04020117.

[47] Guo ZZ, Ma YF, Wang L, Zhang XH, Zhang JR, Hutchinson C, Harik IE. Crack propagation-based fatigue life prediction of corroded RC beams considering bond degradation. Journal of Bridge Engineering, ASCE 2020; 25(8): 04020048.

[48] Lee YJ, Cho S. SHM-based probabilistic fatigue life prediction for bridges based on FE model updating. Sensors 2016; 16(3): 317.

[49] Sun JZ, Ding ZH, Huang Q. Development of EIFS-based corrosion fatigue life prediction

approach for corroded RC beams. Engineering Fracture Mechanics 2019; 209(15): 1-16.

[50] Guo ZZ, Ma YF, Wang L, Zhang JR, Harik IE. Corrosion fatigue crack propagation mechanism of high-strength steel bar in various environments. Journal of Materials in Civil Engineering, ASCE 2020; 32(6): 04020115.

[51] Liang Y, Luo XY, Xiao XQ, Zhang YF. Experimental study on bond-slip performance of corroded RC concrete. Industrial Construction 2012; 42(10): 10-15. (in Chinese)

[52] Molaioni F, Carlo FD, Rinaldi Z. Modelling strategies for the numerical simulation of the behaviour of corroded RC columns under cyclic loads. Applied Sciences 2021; 11(20): 9761.

[53] Georgiou E, Kyriakides N, Chrysostomou C, Kotronis N, Filippou C. Numerical simulation of the experimental results of the seismic strengthening of existing structures. 16th European Conference on Earthquake Engineering, 2018.

[54] Song L, Fan ZW, Hou J. Experimental and analytical investigation of the fatigue flexural behavior of corroded reinforced concrete beams. International Journal of Concrete Structures and Materials 2019; 13(1): 1-14.

[55] Oudah F, El-Hacha R. Research progress on the fatigue performance of RC beams strengthened in flexure using fiber reinforced polymers. Composites Part B: Engineering 2013; 47: 82-95.

[56] Peelen W, Polder R, Redaelli E, Bertolini L. Qualitative model of concrete acidification due to cathodic protection. Materials and Corrosion 2008; 59(2): 81-89.

[57] Chinese Code. Standard for Test Method of Concrete Structures. GB/T 50152-2012, Beijing: China Architecture & Building Press, 2012. (in Chinese).

Notations

a	Length of the gap
a_d	Constant related to the strength of concrete
a_n	Length of the main crack of steel bar after n cycles of cyclic loading
A_s	Initial area of steel bar
$A_s^f(n)$	Area of the most dangerous cross section of steel bar after n cycles of cyclic loading
c	Thickness of concrete protective layer
d_c	Mid-span deflection of C-FRCM pieces subjected to four-point bending at cracking

	load
d_u	Mid-span deflection of C-FRCM pieces subjected to four-point bending at ultimate load
D	Initial diameter of steel bar
E_c	Initial elastic modulus of concrete
$E_s^f(n)$	Modulus of elasticity of concrete after n cycles of fatigue loading
E_t	Stiffness modulus
E_{uc}	Nominal modulus of elasticity of corroded steel bar
E_{u0}	Nominal modulus of elasticity of uncorroded steel bar
f_c	Compressive strength of concrete
f_t	Tensile strength of concrete
f_y	Yield strength of steel bar
f_{yc}	Yield strength of corroded steel bar
f_{y0}	Yield strength of uncorroded steel bar
F_c	Cracking load of C-FRCM subjected to tension
F_u	Ultimate load of C-FRCM subjected to tension
$K_{\max}$	Stress intensity factor corresponding to the upper limit of load
$K_{\min}$	Stress intensity factor corresponding to the lower limit of load
N_{FE}	Fatigue life of beam in FE model
N_i	Fatigue life of concrete
N_{Test}	Fatigue life of beam in experiment
P_c	Cracking load of C-FRCM subjected to four-point bending
$P_{\max}$	Upper limit of load
$P_{\min}$	Lower limit of load
P_u	Ultimate load of C-FRCM subjected to four-point bending
R	Resistance
s_u	Ultimate slip of corroded steel bar
S	Action effect
$S_{\max}$	Maximum load ratio of concrete
$S_{\min}$	Minimum load ratio of concrete

Y	Geometric shape factor
σ	Applied stress
σ_s	Stress of steel bar
$\sigma_{s,max}$	Maximum stress of steel bar
ε_{FE}	Strain of steel bar in FE model
ε_{Test}	Strain of steel bar in experiment
ε_{yc}	Ultimate strain of corroded steel bar
ε_{y0}	Ultimate strain of uncorroded steel bar
δ_c	Nominal elongation of corroded steel bar
δ_{max}	Maximum stress of concrete
$\delta_{r,c}(N)$	Residual strength of concrete under N-th fatigue loading times
δ_0	Nominal elongation of uncorroded steel bar
τ_u	Ultimate bonding strength of corroded steel bar
ρ	Corrosion degree of steel bar
ρ_{sv}	Reinforcement ratio of concrete specimen
$\eta'(\rho)$	Bonding strength reduction coefficient
Δ_{FE}	Deflection of beam in FE model
ΔL_c	Tensile deformation of C-FRCM pieces subjected to four-point bending at cracking load
ΔL_u	Tensile deformation of C-FRCM pieces subjected to four-point bending at ultimate load
ΔS	Magnitude of load ratio on concrete
Δ_{Test}	Deflection of beam in experiment
$\Delta\delta$	Stress amplitude

Group	Specimen	Corrosion	Strengthening	Polarization degree of C-FRCM
1	B-S	N	N	—
2	B-F	N	N	—

	CB-F	Y	N	—
	CSBP0-F	Y	Y	0
	CSBP1-F	Y	Y	1
	CSBP2-F	Y	Y	2

Note: When the polarization degree of C-FRCM is 0, it means that the C-FRCM is not electrified; when the polarization degree of C-FRCM is 1, it means that the C-FRCM is electrified with a current density of 100 mA/m^2 for 90 days; when the polarization degree of C-FRCM is 2, it means that the C-FRCM is electrified with a current density of 150 mA/m^2 for 75 days.

Table 1. Design of test specimens

Tensile test	Specimen	F_c (kN)	ΔL_c (mm)	F_u (kN)	ΔL_u (mm)
	T-P0	4.52	0.049	5.02	1.887
	T-P1	4.44	0.042	4.33	1.640
	T-P2	4.02	0.040	3.56	2.354
Four-point bending test	Specimen	P_c (kN)	d_c (mm)	P_u (kN)	d_u (mm)
	B-P0	0.46	0.750	1.18	14.122
	B-P1	0.44	0.549	0.93	13.193
	B-P2	0.66	0.529	0.55	3.426

Note: C-FRCM pieces with the name of “T-P1” represent that the specimen was subjected to tension, and the polarization degree was 1, while the C-FRCM pieces with the name of “B-P1” represent that the specimen was subjected to four-point bending, and the polarization degree was 1. F_c and ΔL_c are the cracking load and the corresponding tensile deformation of the C-FRCM pieces subjected to tension, while F_u and ΔL_u are the ultimate load and the corresponding tensile deformation of the C-FRCM pieces; P_c and d_c are the cracking load and the corresponding mid-span deflection of C-FRCM pieces subjected to four-point bending, while P_u and d_u are the ultimate load and the corresponding mid-span deflection of C-FRCM pieces.

Table 2. Mechanical property test results of C-FRCM composites

Specimen	Fatigue life (time)	Equivalent initial crack size (mm)
B-F	196,820	0.890
CB-F	117,030	1.295
CSBP0-F	252,856	0.992
CSBP1-F	225,077	1.102
CSBP2-F	145,988	1.297

Table 3. The equivalent initial crack size

Mesh size (mm)	Ultimate load (kN)			Steel bar strain at the mid-span (με)			Steel bar strain at the mid-support (με)			Computing time (s)
	Test m())	FE	F_{Test}/F_{FE}	Test	FE	$\varepsilon_{Test}/\varepsilon_{FE}$	Test	FE	$\varepsilon_{Test}/\varepsilon_{FE}$	
60×60×60	436	455.6	0.957	5794	6162	0.940	5096	5447	0.936	3821
50×50×50	436	442.5	0.985	5794	5957	0.973	5096	5289	0.964	6304
40×40×40	436	442.1	0.986	5794	5950	0.974	5096	5284	0.964	22121
30×30×30	436	442.0	0.986	5794	5946	0.974	5096	5282	0.965	46730

Table 4. Static test simulation result of specimen B-S with varied mesh size

Specimen / Cycle	B-F			CB-F			CSP0B-F			CSP1B-F			CSP2B-F		
	Test	FE	$\Delta_{Test}/\Delta_{FE}$	Test	FE	$\Delta_{Test}/\Delta_{FE}$	Test	FE	$\Delta_{Test}/\Delta_{FE}$	Test	FE	$\Delta_{Test}/\Delta_{FE}$	Test	FE	$\Delta_{Test}/\Delta_{FE}$
0	1.455	1.498	0.971	1.660	1.632	1.017	1.480	1.370	1.080	1.510	1.481	1.020	1.488	1.496	0.995
1,000	1.812	1.545	1.173	2.010	1.788	1.124	1.750	1.478	1.184	1.730	1.596	1.084	1.830	1.560	1.173
5,000	1.881	1.613	1.166	2.030	1.816	1.118	1.760	1.513	1.163	1.750	1.615	1.084	1.944	1.625	1.196
10,000	1.910	1.618	1.180	2.070	1.845	1.122	1.790	1.523	1.175	1.810	1.632	1.109	1.951	1.633	1.195
30,000	1.920	1.683	1.141	2.110	1.937	1.089	1.814	1.547	1.172	1.850	1.655	1.118	1.977	1.697	1.165
50,000	1.980	1.720	1.151	2.130	1.992	1.069	1.865	1.566	1.191	1.890	1.686	1.121	1.980	1.718	1.153
100,000	2.030	1.825	1.112	2.260	2.198	1.028	1.910	1.637	1.167	1.910	1.743	1.096	2.067	1.842	1.122
200,000	—	—	—	—	—	—	2.020	1.825	1.107	2.150	1.970	1.091	—	—	—
Mean			1.128			1.081			1.155			1.090			1.143
COV			0.060			0.038			0.032			0.027			0.057

Table 5. Mid-span deflections of RC continuous beams (mm)

Specimen / Cycle	B-F			CB-F			CSP0B-F			CSP1B-F			CSP2B-F		
	Test	FE	$\varepsilon_{Test}/\varepsilon_{FE}$	Test	FE	$\varepsilon_{Test}/\varepsilon_{FE}$	Test	FE	$\varepsilon_{Test}/\varepsilon_{FE}$	Test	FE	$\varepsilon_{Test}/\varepsilon_{FE}$	Test	FE	$\varepsilon_{Test}/\varepsilon_{FE}$
0	1651	1540	1.072	—	—	—	1442	1533	0.941	1532	1536	0.997	1565	1567	0.999
1,000	1755	1598	1.098	1940	1945	0.997	1658	1597	1.038	1562	1597	0.978	1657	1658	0.999
5,000	1758	1605	1.095	1965	1945	1.010	1700	1605	1.059	1682	1613	1.043	1661	1662	0.999
10,000	1758	1614	1.089	2011	1947	1.033	1739	1609	1.081	1684	1618	1.041	1667	1667	1.000
30,000	1757	1626	1.081	2010	1953	1.029	1799	1616	1.113	1728	1628	1.061	1675	1677	0.999

50,000	1753	1632	1.074	2025	1961	1.033	1822	1638	1.112	1751	1635	1.071	1677	1678	0.999
100,000	1754	1634	1.073	2192	1973	1.111	1878	1645	1.142	1768	1638	1.079	1686	1687	0.999
200,000	1756	1635	1.074	—	—	—	1863	1663	1.120	1825	1643	1.111	—	—	—
Mean			1.082			1.036			1.076			1.048			0.999
COV			0.009			0.035			0.056			0.039			0.000

Table 6. Steel bar strains at the mid-span of RC continuous beams (με)

Specimen / Cycle	B-F			CB-F			CSP0B-F			CSP1B-F			CSP2B-F		
	Test	FE	$\varepsilon_{Test}/\varepsilon_{FE}$	Test	FE	$\varepsilon_{Test}/\varepsilon_{FE}$	Test	FE	$\varepsilon_{Test}/\varepsilon_{FE}$	Test	FE	$\varepsilon_{Test}/\varepsilon_{FE}$	Test	FE	$\varepsilon_{Test}/\varepsilon_{FE}$
0	1563	1650	0.947	—	—	—	1196	1655	0.723	1651	1647	1.002	1702	1657	1.027
1,000	1634	1752	0.933	1924	2003	0.961	1292	1740	0.743	1772	1748	1.014	1788	1758	1.017
5,000	1632	1752	0.932	1957	2004	0.977	1443	1744	0.827	1765	1749	1.009	1789	1763	1.015
10,000	1635	1758	0.930	2006	2005	1.000	1568	1746	0.898	1795	1751	1.025	1799	1767	1.018
30,000	1643	1756	0.936	2052	2006	1.023	1615	1748	0.924	1785	1750	1.020	1798	1777	1.012
50,000	1645	1760	0.935	2055	2008	1.023	1641	1753	0.936	1798	1755	1.025	—	—	—
100,000	1668	1754	0.951	2112	2011	1.050	1712	1758	0.974	1800	1761	1.022	—	—	—
200,000	1715	1756	0.977	—	—	—	1766	1765	1.001	1810	1765	1.025	—	—	—
Mean			0.942			1.006			0.878			1.018			1.018
COV			0.016			0.030			0.110			0.008			0.005

Table 7. Steel bar strains at the mid-support of RC continuous beams (με)

Specimen	N_{Test} (time)	N_{FE} (time)	N_{Test}/N_{FE}
B-F	196,820	215,256	0.914
CB-F	117,000	121,452	0.963
CSBP0-F	252,856	284,251	0.890
CSBP1-F	225,077	254,337	0.885
CSBP2-F	145,988	158,224	0.923
Mean			0.915
COV			0.031

Table 8. Comparison of fatigue life of RC continuous beams in tests and FE model

Corrosion degree (%)	Fatigue life N ($\times 10^4$)	Fatigue load P_{min}/P_{max} (kN)	Applied load ratio P_{max}/P_y	Strengthening	Reference
0	273.4	10/35	0.515(35/68)	No	Song and Yu [24]
4.7	96.8	10/35	0.515(35/68)	No	
8.1	53.7	10/35	0.515(35/68)	No	
8.3	134.6	10/35	0.515(35/68)	Yes	
13.8	45.9	10/35	0.515(35/68)	Yes	
0	26.5	10.54/85.6	0.65(85.6/131.73)	No	Al-Hammoud et al. [21]
4.6	32.6	10.54/85.6	0.65(85.6/131.73)	No	
7.8	38.7	10.54/85.6	0.65(85.6/131.73)	Yes	
12.8	17.8	10.54/85.6	0.65(85.6/131.73)	Yes	

Table 9. Fatigue test results of corroded RC beams

Specimen	Corrosion degree of steel bar (%)	Load level	Polarization degree of C-FRCM	Fatigue life (time)
C0B-L0.2	0	0.2	—	1,580,759
C0B-L0.3	0	0.3	—	937,365
C0B-L0.4	0	0.4	—	518,538
C0B-L0.5	0	0.5	—	300,137
C0B-L0.6	0	0.6	—	179,477
C3.5B-L0.2	3.5	0.2	—	1,154,249

C3.5B-L0.3	3.5	0.3	—	679,577
C3.5B-L0.4	3.5	0.4	—	384,713
C3.5B-L0.5	3.5	0.5	—	227,513
C3.5B-L0.6	3.5	0.6	—	116,296
C7B-L0.2	7	0.2	—	913,941
C7B-L0.3	7	0.3	—	534,782
C7B-L0.4	7	0.4	—	283,201
C7B-L0.5	7	0.5	—	157,611
C7B-L0.6	7	0.6	—	84,275
C0SP0B-L0.2	0	0.2	0	2,590,252
C0SP0B-L0.3	0	0.3	0	1,545,775
C0SP0B-L0.4	0	0.4	0	766,716
C0SP0B-L0.5	0	0.5	0	414,674
C0SP0B-L0.6	0	0.6	0	225,275
C3.5SP0B-L0.2	3.5	0.2	0	2,075,357
C3.5SP0B-L0.3	3.5	0.3	0	1,233,852
C3.5SP0B-L0.4	3.5	0.4	0	611,396
C3.5SP0B-L0.5	3.5	0.5	0	319,707
C3.5SP0B-L0.6	3.5	0.6	0	173,386
C7SP0B-L0.2	7	0.2	0	1,641,032
C7SP0B-L0.3	7	0.3	0	971,428
C7SP0B-L0.4	7	0.4	0	478,691
C7SP0B-L0.5	7	0.5	0	256,791
C7SP0B-L0.6	7	0.6	0	134,165
C0SP1B-L0.2	0	0.2	1	2,159,863
C0SP1B-L0.3	0	0.3	1	1,421,521
C0SP1B-L0.4	0	0.4	1	718,325
C0SP1B-L0.5	0	0.5	1	393,434
C0SP1B-L0.6	0	0.6	1	215,841
C3.5SP1B-L0.2	3.5	0.2	1	1,733,972
C3.5SP1B-L0.3	3.5	0.3	1	1,135,733
C3.5SP1B-L0.4	3.5	0.4	1	573,147
C3.5SP1B-L0.5	3.5	0.5	1	303,585
C3.5SP1B-L0.6	3.5	0.6	1	175,368
C7SP1B-L0.2	7	0.2	1	1,373,928
C7SP1B-L0.3	7	0.3	1	894,319
C7SP1B-L0.4	7	0.4	1	449,142
C7SP1B-L0.5	7	0.5	1	241,620
C7SP1B-L0.6	7	0.6	1	128,615
C0SP2B-L0.2	0	0.2	2	1,997,151
C0SP2B-L0.3	0	0.3	2	1,310,680
C0SP2B-L0.4	0	0.4	2	674,048

C0SP2B-L0.5	0	0.5	2	373,657
C0SP2B-L0.6	0	0.6	2	206,855
C3.5SP2B-L0.2	3.5	0.2	2	1,604,810
C3.5SP2B-L0.3	3.5	0.3	2	1,048,096
C3.5SP2B-L0.4	3.5	0.4	2	489,479
C3.5SP2B-L0.5	3.5	0.5	2	289,435
C3.5SP2B-L0.6	3.5	0.6	2	159,182
C7SP2B-L0.2	7	0.2	2	1,275,256
C7SP2B-L0.3	7	0.3	2	827,836
C7SP2B-L0.4	7	0.4	2	422,201
C7SP2B-L0.5	7	0.5	2	231,933
C7SP2B-L0.6	7	0.6	2	123,422

Table 10. Fatigue life of RC continuous beams in parametric study

Specimen	Curve expression	R^2
C0B	$\lg N=-1.977\lg S+9.888$	0.976
C3.5B	$\lg N=-2.035\lg S+9.866$	0.962
C7B	$\lg N=-2.141\lg S+9.977$	0.984
C0SP0B	$\lg N=-2.224\lg S+10.575$	0.967
C3.5SP0B	$\lg N=-2.264\lg S+10.555$	0.965
C7SP0B	$\lg N=-2.272\lg S+10.467$	0.965
C0SP1B	$\lg N=-2.103\lg S+10.284$	0.955
C3.5SP1B	$\lg N=-2.112\lg S+10.199$	0.958
C7SP1B	$\lg N=-2.157\lg S+10.186$	0.976
C0SP2B	$\lg N=-2.068\lg S+10.182$	0.956
C3.5SP2B	$\lg N=-2.142\lg S+10.204$	0.960
C7SP2B	$\lg N=-2.120\lg S+10.087$	0.954

Table 11. *S*-*N* curve expression

Specimen / Load level	C0B	C3.5B	C7B	C0SP0B	C3.5SP0B	C7SP0B	C0SP1B	C3.5SP1B	C7SP1B	C0SP2B	C3.5SP2B	C7SP2B
0.2	100.0	100.0	100.0	100.0	100.0	100.0	100.0	100.0	100.0	100.0	100.0	100.0
0.3	59.3	58.9	58.5	59.7	59.5	59.2	65.8	65.5	65.1	65.6	65.3	64.9
0.4	32.8	33.3	31.0	29.6	29.5	29.2	33.3	33.1	32.7	33.8	30.5	33.1
0.5	19.0	19.7	17.2	16.0	15.4	15.6	18.2	17.5	17.6	18.7	18.0	18.2
0.6	11.4	10.1	9.2	8.7	8.4	8.2	10.0	10.1	9.4	10.4	9.9	9.7

Table 12. Fatigue life ratio under different load levels (%)

Specimen / Corrosion degree	B -L0.2	B -L0.3	B -L0.4	B -L0.5	B -L0.6	SP0B -L0.2	SP0B -L0.3	SP0B -L0.4	SP0B -L0.5	SP0B -L0.6	SP1B -L0.2	SP1B -L0.3	SP1B -L0.4	SP1B -L0.5	SP1B -L0.6	SP2B -L0.2	SP2B -L0.3	SP2B -L0.4	SP2B -L0.5	SP2B -L0.6
0	100	100	100	100	100.0	100.0	100.0	100.0	100.0	100.0	100.0	100.0	100.0	100.0	100.0	100.0	100.0	100.0	100.0	100.0
3.5	73.0	72.5	74.2	75.8	64.8	80.1	79.8	79.7	77.1	77.0	80.3	79.9	79.8	77.2	81.2	80.4	80.0	72.6	77.5	77.0
7	57.8	57.1	54.6	52.5	47.0	63.4	62.8	62.4	61.9	59.6	63.6	62.9	62.5	61.4	59.6	63.9	63.2	62.6	62.1	59.7

Table 13. Fatigue life ratio under different corrosion degrees of steel bar (%)

Specimen / Polarization degree	C0SB -L0.2	C0SB -L0.3	C0SB -L0.4	C0SB -L0.5	C0SB -L0.6	C3.5SB -L0.2	C3.5SB -L0.3	C3.5SB -L0.4	C3.5SB -L0.5	C3.5SB -L0.6	C7SB -L0.2	C7SB -L0.3	C7SB -L0.4	C7SB -L0.5	C7SB -L0.6
0	100.0	100.0	100.0	100.0	100.0	100.0	100.0	100.0	100.0	100.0	100.0	100.0	100.0	100.0	100.0
1	83.4	92.0	93.7	94.9	95.8	83.6	92.0	93.7	95.0	101.1	83.7	92.1	93.8	94.1	95.9
2	77.1	84.8	87.9	90.1	91.8	77.3	84.9	80.1	90.5	91.8	77.7	85.2	88.2	90.3	92.0

Table 14. Fatigue life ratio under different polarization degrees of C-FRCM (%)

Specimen \ Cycle	0	10,000	50,000	100,000	200,000	500,000	1,000,000	2,000,000
C0B-L0.2	1.000	1.000	0.999	0.998	0.984	0.949	0.685	0.508
C0B-L0.3	1.000	0.999	0.997	0.988	0.875	0.592	0.278	0.125
C0B-L0.4	1.000	0.998	0.986	0.918	0.652	0.304	0.213	0.102
C0B-L0.5	1.000	0.984	0.938	0.808	0.400	0.215	0.153	0.054
C0B-L0.6	1.000	0.949	0.833	0.598	0.206	0.0545	0.0521	0.028
C3.5B-L0.2	1.000	1.000	0.998	0.991	0.931	0.686	0.511	0.358
C3.5B-L0.3	1.000	0.996	0.987	0.953	0.749	0.454	0.255	0.148
C3.5B-L0.4	1.000	0.989	0.969	0.870	0.502	0.217	0.110	0.068
C3.5B-L0.5	1.000	0.987	0.948	0.840	0.452	0.190	0.100	0.054
C3.5B-L0.6	1.000	0.851	0.670	0.403	0.119	0.039	0.012	0.003
C7B-L0.2	1.000	0.997	0.986	0.974	0.850	0.576	0.387	0.262
C7B-L0.3	1.000	0.989	0.982	0.921	0.672	0.456	0.336	0.198
C7B-L0.4	1.000	0.973	0.919	0.759	0.365	0.214	0.141	0.032
C7B-L0.5	1.000	0.891	0.765	0.536	0.187	0.050	0.050	0.011
C7B-L0.6	1.000	0.786	0.618	0.313	0.070	0.01	0.005	0.001
C0SP0B-L0.2	1.000	1.000	1.000	0.998	0.973	0.8385	0.685	0.508
C0SP0B-L0.3	1.000	1.000	1.000	0.999	0.970	0.811	0.654	0.489
C0SP0B-L0.4	1.000	0.998	0.997	0.975	0.818	0.496	0.293	0.187
C0SP0B-L0.5	1.000	0.997	0.976	0.880	0.542	0.230	0.117	0.069
C0SP0B-L0.6	1.000	0.976	0.906	0.682	0.282	0.082	0.028	0.013
C3.5SP0B-L0.2	1.000	1.000	0.999	0.997	0.978	0.890	0.724	0.564
C3.5SP0B-L0.3	1.000	1.000	0.998	0.989	0.915	0.716	0.516	0.383
C3.5SP0B-L0.4	1.000	0.997	0.951	0.943	0.745	0.378	0.225	0.143
C3.5SP0B-L0.5	1.000	0.982	0.950	0.812	0.44	0.161	0.075	0.039
C3.5SP0B-L0.6	1.000	0.930	0.811	0.569	0.197	0.048	0.029	0.013
C7SP0B-L0.2	1.000	1.000	0.999	0.990	0.964	0.835	0.657	0.543
C7SP0B-L0.3	1.000	0.997	0.992	0.978	0.845	0.597	0.445	0.294
C7SP0B-L0.4	1.000	0.990	0.962	0.891	0.611	0.308	0.157	0.098
C7SP0B-L0.5	1.000	0.955	0.880	0.728	0.313	0.110	0.051	0.029
C7SP0B-L0.6	1.000	0.894	0.740	0.469	0.134	0.033	0.018	0.009
C0SP1B-L0.2	1.000	1.000	1.000	1.000	0.987	0.920	0.735	0.564
C0SP1B-L0.3	1.000	1.000	1.000	0.999	0.951	0.786	0.603	0.447
C0SP1B-L0.4	1.000	1.000	0.996	0.9715	0.799	0.452	0.259	0.164
C0SP1B-L0.5	1.000	0.996	0.978	0.884	0.550	0.2215	0.101	0.067
C0SP1B-L0.6	1.000	0.975	0.901	0.676	0.266	0.081	0.039	0.019
C3.5SP1B-L0.2	1.000	1.000	1.000	0.997	0.982	0.884	0.652	0.521

C3.5SP1B-L0.3	1.000	1.000	0.997	0.989	0.918	0.714	0.516	0.377
C3.5SP1B-L0.4	1.000	0.997	0.989	0.948	0.745	0.424	0.222	0.135
C3.5SP1B-L0.5	1.000	0.978	0.938	0.812	0.431	0.161	0.070	0.037
C3.5SP1B-L0.6	1.000	0.930	0.816	0.570	0.192	0.048	0.017	0.005
C7SP1B-L0.2	1.000	1.000	0.999	0.994	0.961	0.823	0.665	0.532
C7SP1B-L0.3	1.000	0.997	0.992	0.973	0.863	0.607	0.425	0.305
C7SP1B-L0.4	1.000	0.986	0.968	0.883	0.598	0.291	0.160	0.111
C7SP1B-L0.5	1.000	0.863	0.725	0.456	0.146	0.033	0.015	0.009
C7SP1B-L0.6	1.000	0.966	0.899	0.728	0.327	0.134	0.015	0.009
C0SP2B-L0.2	1.000	1.000	1.000	0.998	0.973	0.839	0.655	0.508
C0SP2B-L0.3	1.000	1.000	1.000	0.998	0.932	0.762	0.552	0.405
C0SP2B-L0.4	1.000	0.998	0.995	0.968	0.780	0.408	0.225	0.140
C0SP2B-L0.5	1.000	0.995	0.976	0.880	0.542	0.213	0.086	0.065
C0SP2B-L0.6	1.000	0.975	0.896	0.669	0.250	0.080	0.028	0.000
C3.5SP2B-L0.2	1.000	1.000	1.000	0.996	0.978	0.878	0.639	0.532
C3.5SP2B-L0.3	1.000	1.000	0.995	0.989	0.915	0.713	0.516	0.371
C3.5SP2B-L0.4	1.000	0.997	0.977	0.943	0.745	0.378	0.220	0.126
C3.5SP2B-L0.5	1.000	0.974	0.926	0.811	0.422	0.161	0.064	0.036
C3.5SP2B-L0.6	1.000	0.930	0.811	0.569	0.186	0.048	0.006	0.000
C7SP2B-L0.2	1.000	1.000	0.999	0.99	0.9585	0.8115	0.657	0.522
C7SP2B-L0.3	1.000	0.997	0.992	0.969	0.845	0.597	0.404	0.294
C7SP2B-L0.4	1.000	0.982	0.962	0.876	0.585	0.274	0.157	0.098
C7SP2B-L0.5	1.000	0.953	0.856	0.650	0.325	0.125	0.075	0.034
C7SP2B-L0.6	1.000	0.894	0.740	0.469	0.134	0.033	0.013	0.009

Table 15. Fatigue life reliability of RC continuous beams in parametric study

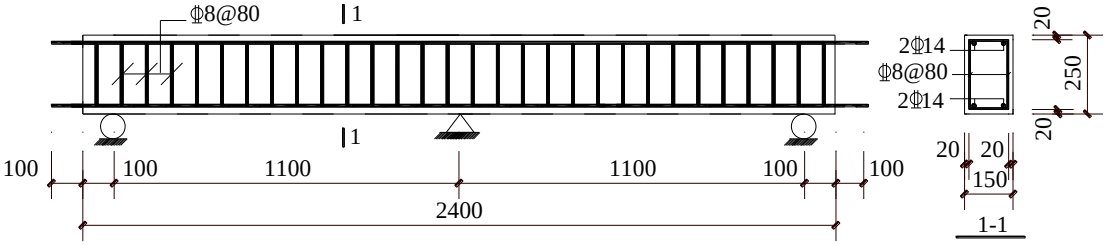

Figure 1. Steel bar configuration of RC continuous beams

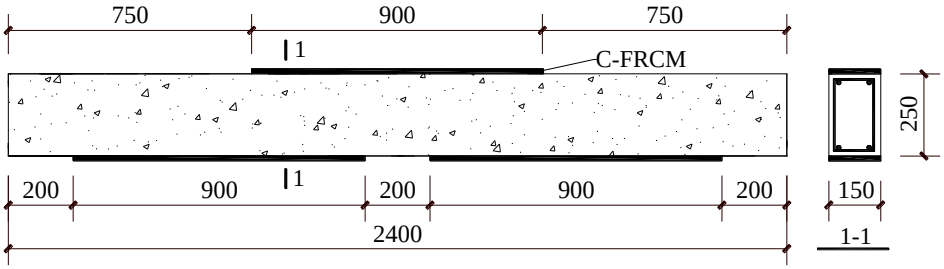

Figure 2. Strengthening area of RC continuous beams

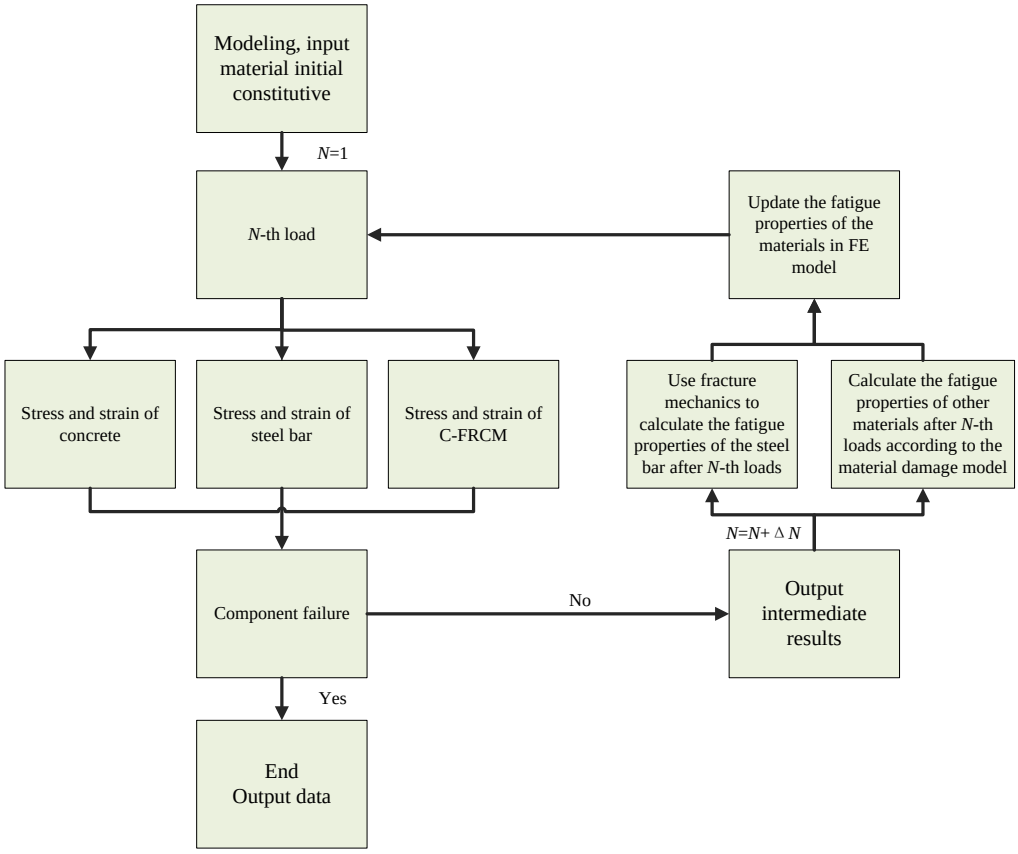

Figure 3. Analysis chart of the fatigue life prediction model of RC continuous beams

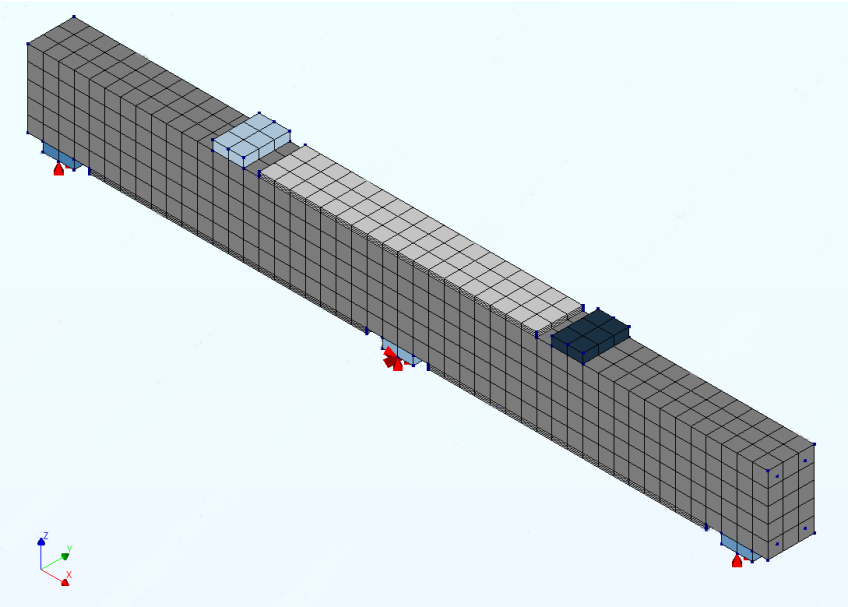

Figure 4. FE model of RC continuous beams

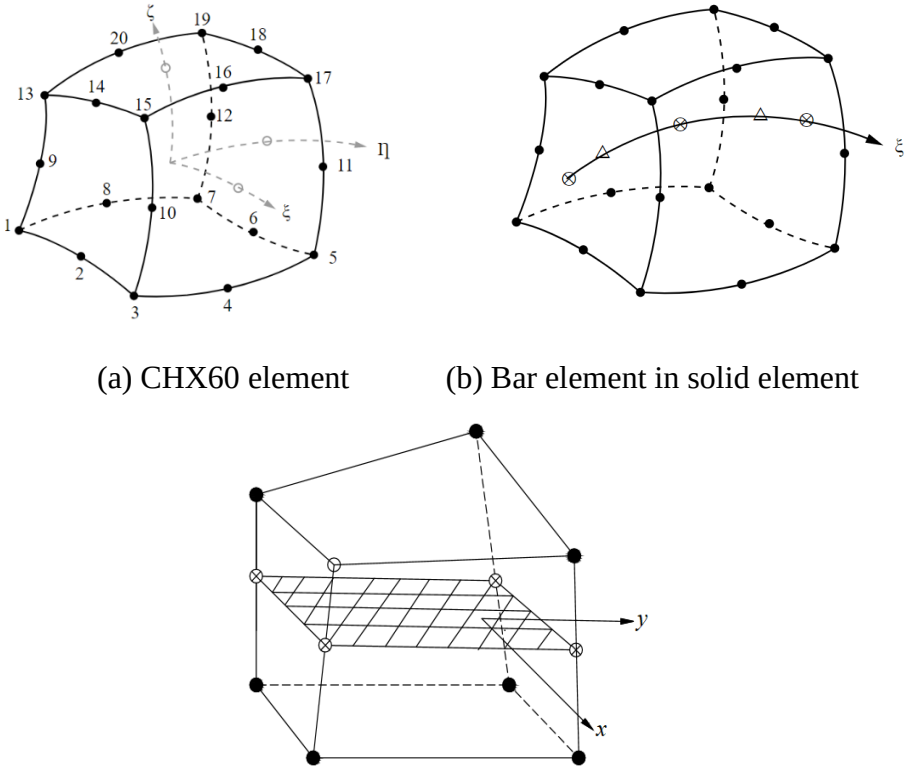

(a) CHX60 element (b) Bar element in solid element

(c) Grid element in solid element

Figure 5. Related elements of fatigue life prediction model

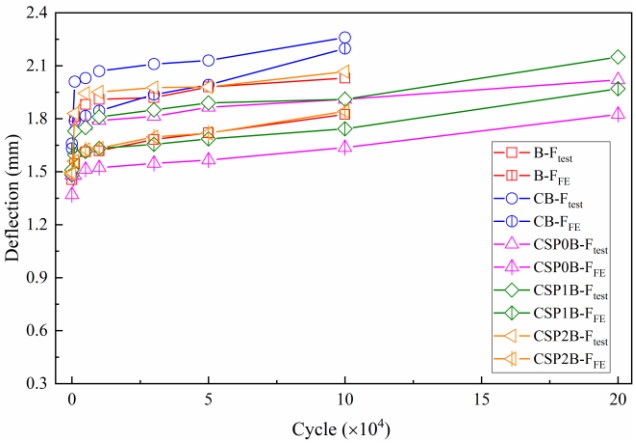

(a) Deflection at mid-span of RC beams

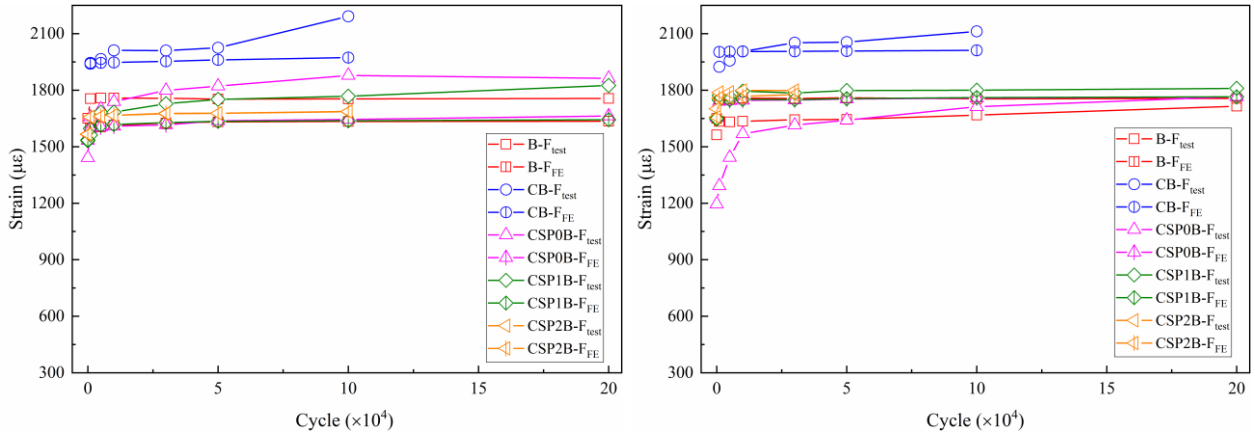

(b) Steel bar strain at mid-span of RC beams (c) Steel bar strain at mid-support of RC beams

Figure 6. Comparison of test and FE results

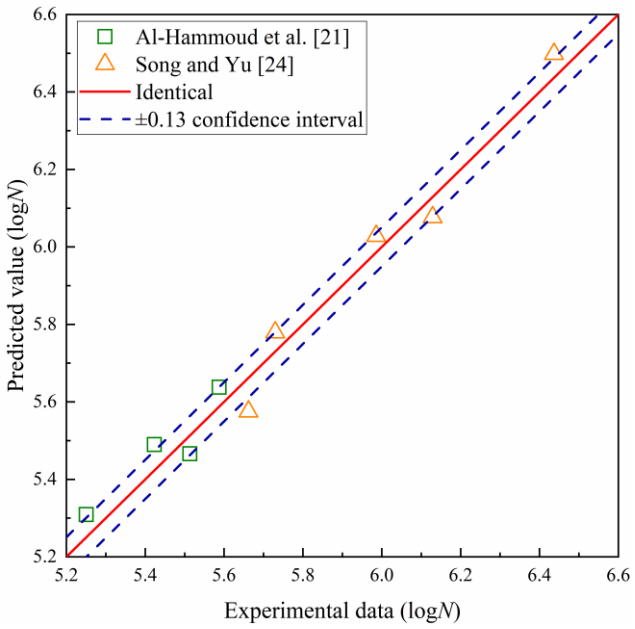

Figure 7. Comparison between predictions and test data

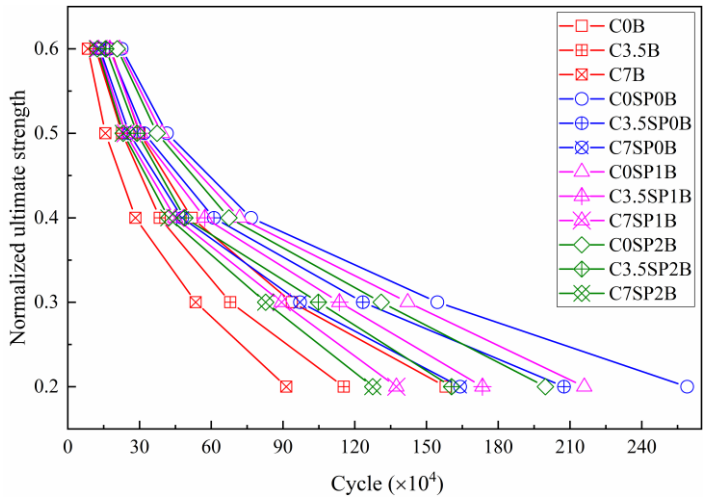

Figure 8. Load amplitude versus fatigue life curves

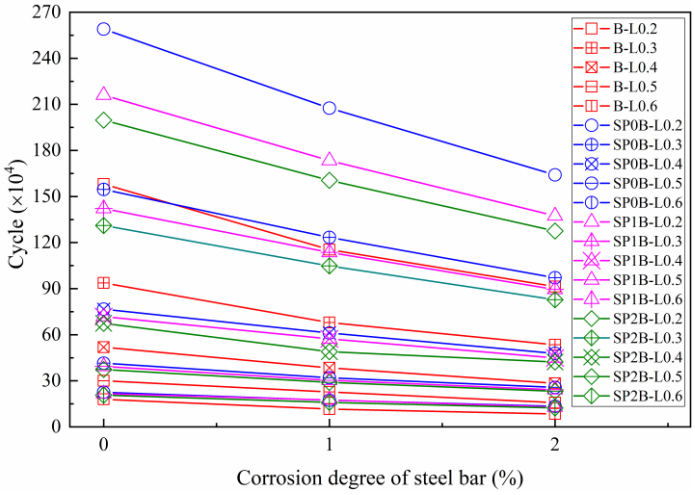

Figure 9. Corrosion degree of steel bar versus fatigue life curves

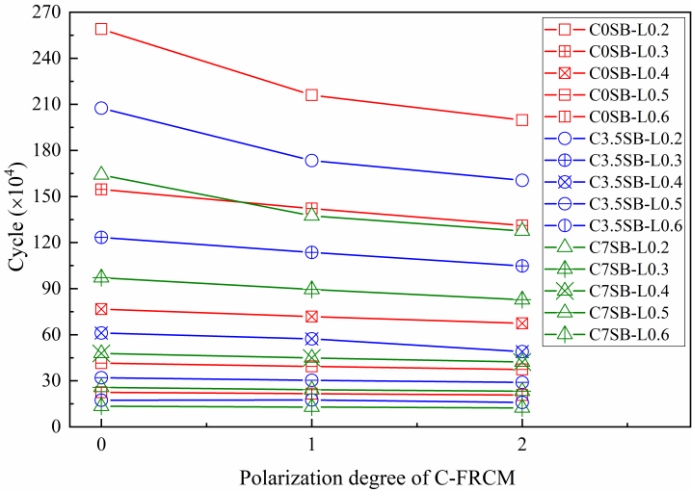

Figure 10. Polarization degree of C-FRCM versus fatigue life curves

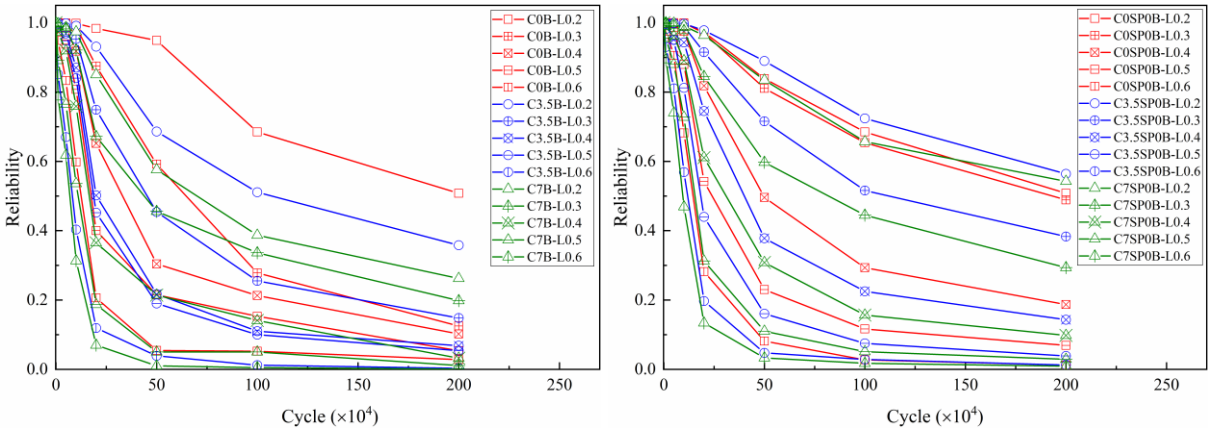

(a) B series (b) SP0B series

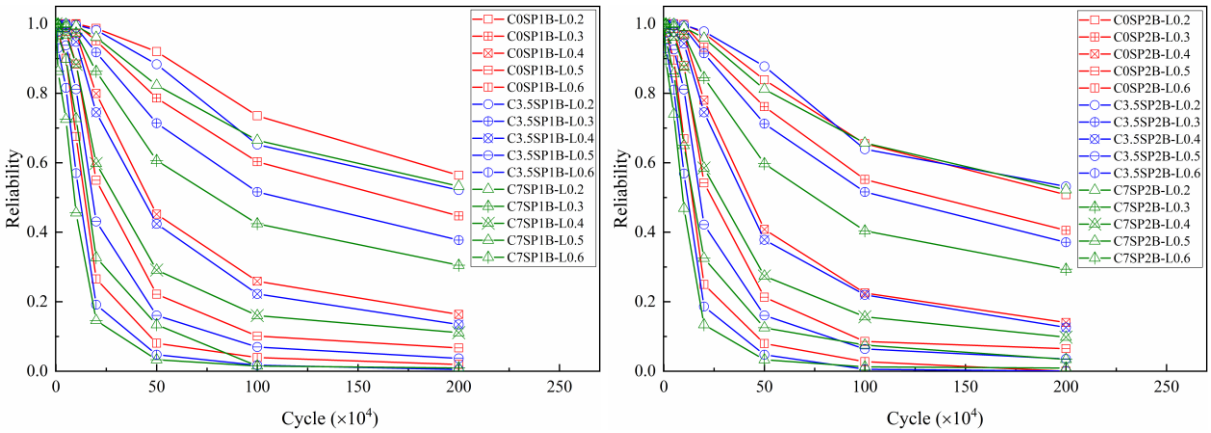

(c) SP1B series (d) SP2B series

Figure 11. Fatigue life reliability curves of RC continuous beams in parametric study